

POLITECNICO DI MILANO

Scuola di Ingegneria Industriale e dell'Informazione

Corso di Laurea Magistrale in
Engineering Physics



Simulation of Montel system

Relatore: Prof. Giacomo GHIRINGHELLI

Correlatore: Dott. Manuel SANCHEZ DEL RIO

Tesi di Laurea di:

Yiones AOUADI Matr. 872727

Anno Accademico 2017 - 2018

Yiones Aouadi: *Modello di Tesi di Laurea in L^AT_EX* | Tesi di Laurea Magistrale in
Engineering physics, Politecnico di Milano.
© Copyright Dicembre 2018.

Politecnico di Milano:
www.polimi.it

Scuola di Ingegneria Industriale e dell'Informazione:
www.ingindinf.polimi.it

*a te,
ovunque tu sia,
e qualunque percorso di vita tu abbia intrapreso.*

Indice

Introduzione	1
1 Focusing for X-rays	3
1.1 Interaction with Matter	5
1.2 Total External Reflection	9
2 Mirrors for X-rays	15
2.1 Spherical surface	15
2.1.1 Astigmatism	15
2.1.2 Spherical Aberration	17
2.1.3 Reducing aberration	18
2.2 Conic Surfaces	18
2.3 Compound Optical system	19
2.3.1 Wolter System [SS05]	20
2.3.2 Kirkpatrick-Baez System [MY09]	21
2.4 Montel	22
2.4.1 Description	22
2.4.2 Optical Design [IBK09]	23
3 MONWES	25
3.1 Beam	25
3.2 Optical Elements	29
3.2.1 Mirrors and lens	29
3.2.2 Compound Optical Element (KB and Montel system)	33
3.2.3 Compound System: KirkPatrickBaez	33
3.2.4 Compound System: Montel	34
3.3 Tracing System	35
3.3.1 Tracing for simple Optical element	36
3.3.2 Tracing for KB	37
3.3.3 Tracing for Montel	37
4 Test and Results	41
4.1 Testing against OASYS	41
4.1.1 Benchmarking	44
4.2 Analysis of Montel system	44
4.3 Non-centred Beam	47
4.4 My work for the ID 20	51

4.4.1	System parameters	51
4.4.2	Result of beam figure and footprint	52
4.4.3	Analysis of orthogonality	52
A	Table for absorption coefficents	55
B	How to calculated the ellipse's and hyperbola's coefficients	59

Elenco delle figure

1.1	Attenuation coefficient for X-ray radiation of a light material (water Figure 1.1a), and an heavy material (lead 1.1b) (from [SFV09]).	4
1.2	X-ray ionizing process	6
1.3	Interface of two medium	9
1.4	Reflectivity for the case of a non-absorbing material	13
1.5	Reflectivity plot with respect of the grazing incidence angle ϑ_i of different material with a radiation of 500eV on a substrate of Si [LBN10]	14
2.1	Formation image of a circular mirror for a point-wise source placed at a distance PO from the center of the mirror. R is the curvature of the mirror, ϑ_i the angle of the central ray.	16
2.2	Image formation of a spherical mirror. The formation of a point wise source correspond to a two rods, one in the sagittal plane, and the second one in the meridial plane	17
2.3	Different kind of surface conic, with the same c base curvature value, and different constant k	19
2.4	Example of spherical aberration correction	20
2.5	Sine Abbe condition for a lens	20
2.6	Kirkpatrick-Baez system	22
2.7	Montel system	23
2.8	Example in how to build a Montel system starting from two cylindrical mirror cutting the edge with ad angle of 45°.	24
3.1	Example of Beam initialization	26
3.2	Example 1	26
3.3	Example 2	27
3.4	Example 3	27
3.5	Summary of the Beam object parameter	28
3.6	Parabola	30
3.7	Part of a parabola (blue), with other characteristic (different color) [Wik18]	31
3.8	Ellipse System	32
3.9	Hyperbola System	32
3.10	KB system	33

3.11	Different object/image focal length that characterize the whole KB system, and the single mirrors. Is it also showed the separation length between the two mirror	34
3.12	Example 5	34
3.13	System	35
3.14	Example 6	35
3.15	System	36
3.16	Example 7	36
3.17	Example 1	37
3.18	Example 8	37
3.19	From [LIA ⁺ 11]. For the KB system (Figure 3.19a) all the rays hit sequentially one mirror after the other. For the Montel system (Figure 3.19b) a portion of rays coming from the source hit firstly oe1 and secondly oe2, the other portion do the opposite thing.	38
3.20	Example 8	39
3.21	Example 8	40
4.1	Optical system used for the test with OASYS	42
4.2	Parameter of the source used for the test with OASYS	42
4.3	Image for the testing ideal lenses system in Figure 4.1 of: my simulation (Figure 4.3a) and OASYS simulation (Figure 4.3b)	43
4.4	Image for the testing paraboloid system in Figure 4.1 of: my simulation (Figure 4.4a) and OASYS simulation (Figure 4.4b)	43
4.5	Image for the testing KB system in Figure 4.1 of: my simulation (Figure 4.5a) and OASYS simulation (Figure 4.5b)	43
4.6	Illustration of the Montel system used as a collimator in the paper [RKM15]	44
4.7	Results of the Montel simulations with a source beam with a FWHM spot of $2.5\mu\text{m}$ and a Gaussian divergence of 5mrad	45
4.8	Ideal system	46
4.9	Illumination at the image plane of the different Beam (red dots correspond to np-reflected rays, blue dot to one-reflected rays, green dots to two-reflected rays).	47
4.10	Different path for simulate the non-centred beam	48
4.11	Results of the Montel system of a source beam with a FWHM spot of $2.5\mu\text{m}$ and a Gaussian divergence of 5mrad	49
4.12	Results of the Montel system of a source beam with a FWHM spot of $2.5\mu\text{m}$ and a Gaussian divergence of 5mrad	50
4.13	Source parameters used for the study of the Montel Analyser for ID20	51
4.14	Montel parameters used for the simulation for ID20	51
4.15	Footprint, on the xy-mirror (4.15c) and on zy-mirror (4.15d). The red dots are those rays that hit before xy-mirror and after zy-mirror, the blue ones hit first xy-mirror and after zy-mirror.	52
4.16	FWHM of x' after the Montel changing the orthogonality	53
4.17	Histogram of x' after Montel	54
B.1	Hyperbola's system	60

B.2 Hyperbola's system 61

Elenco delle tabelle

2.1 Parameter of different conic surfaces	19
---	----

Elenco dei codici

Sommario

La simulazione delle proprietà di fasci di raggi X lungo la propagazione nelle beamline, è uno step importante per la progettazione e l'ottimizzazione di esse. Per sistemi ottici basati sulla riflessione singoli specchi o particolari combinazioni di specchi vengono utilizzati per la focalizzazione del fascio. Un esempio tipico di questi sistemi è il sistema KirckPatrick-Baez (KB), molto popolare all'ESRF per le sue molteplici qualità. Comunque, siccome la qualità dei fasci generata dal sincrotrone dell'ESRF è molto elevata, si va sempre più alla ricerca di elementi ottici via via migliori.

Durante il mio periodo di tirocinio all'ESRF, ho sviluppato una libreria python, in grado di simulare la propagazione di fasci attraverso semplici specchi sferici, e combinazioni di essi quali il sopracitato KirckPatrick-Baez e un altro sistema, denominato Montel. Lo scopo della tesi è stato quello di studiare il sistema Montel utilizzando la libreria generata.

Abstract

The simulation of x-ray beam properties during the transport along a beamline is important for the design, the optimization and the operation of the beamline. For reflection optical system single mirrors or particular combination of them are used to increase the focusing property of a beam. A typical example is the Kirkpatrick-Baez (KB) system, very popular at the ESRF because of its many good properties and so well studied. However, the extreme quality of the synchrotron beams that will be available with the ESRF upgraded storage ring pushes the requirement in optics to consider more and more perfect elements.

During my trainership period at ESRF, I developed a python library in able to simulate a beam propagation along simple surface conic mirrors, and combination of them such as the already discussed KirckPatrick-Baez and another system, named Montel. The aim of the thesis was that to study the effect of Montel system using the builded library.

Introduzione

The simulation of x-ray beam properties during the transport along a beamline is important for the design, the optimization and the operation of the beamline. The main optical element used for X-ray are curved mirrors, used in a grazing configuration, in order to focalize or collimate a beam. In a beam line are used simple mirrors or some particular kind of mirror combination that increase the performance of the optical system. An typical example is the Kirkpatrick-Baez (KB) system, very popular at the ESRF because of its many good properties and so well studied. However, the extreme quality of the synchrotron beams that will be available with the ESRF upgraded storage ring pushes the requirement in optics to consider more and more perfect elements. There is also another configuration of mirror, named "Montel" system, that should do the same work of the Kirkpatrick-Baez (KB) system.

During my traineeships at the ESRF I developed a python library that is able to simulate a ray-tracing of a beam to some simple optical element, such as mirror, and other a bit complicated that are basically a combination of mirrors element such as Kirkpatrick-Baez (KB) system and a Montel system.

Moreover the Montel code it is used to understand the effect of such element with respect to an incident beam in order to

The thesis is struchter in

1. Chapter 1: review of the interaction x-ray - matter in order to explain the importance of the mirror in a grazing configuration for x-ray radiation
2. Chapter 2: it is reported the theoretical explanation of mirror effect, and it is done a study of the Kirkpatrick-Baez (KB) system and Montel system, with a comparison between them.
3. Chapter 4: describes how the python library works going defining the way in which the algoritm is written
4. Chapter 5: shows the correct operation of the program testing it with respect to OASYS, software developed by Manuel Sanchez Del Rio, end a paper. Then report the analysis of Montel simulation done.

Capitolo 1

Focusing for X-rays

Image formation by an optical system usually implies some form of focusing. Moreover the environment in which the radiation it's surrounded, such as the material of which a certain mirror is made, controls the focusing property. In case of the visible light the focusing elements mainly used are lenses with their laws, well-known and studied, for the electron focusing, the optical element become electric and magnetic fields that to curve the path of the electrons. To study the focusing property of the X-ray radiation, it have to consider the interaction that acts between the radiation and the matter. These phenomena are, that rule the interaction radiation-matter are:

1. elastic scattering;
2. inelastic scattering;
3. absorption via photoelectric effect.

The first effect, where there is an exchange of energy, is constituted by: Thomson scattering, that it is the scattering of electromagnetic radiation by a free non relativistic charged particle [Dal16], and Rayleigh scattering, an elastic scattering between the radiation and the strongly bounded electrons that act cooperatively [Fit06]. Because, the elastic scattering, generated a defned phase relation beetwen the incident and the scattered radiation, it is the responsible of Bragg diffraction. The second effect ,inelastic scattering, or Compton scattering [Uni16], that occurs when an electron lost by the atom interact with the radiation and absorb a small energy from the X-ray radiation. This scattering is an incoherent effect so there isn't any phase relation between incident and scattered radiation, moreover the atom pass to another quantum state due to the energy absorbed by the electron. The last effect, absorption via photoelectric effect, occur when an bounded electron with an atom get the necessary energy to break the bound and become free (ionization process). This last phenomenon is the most important effet fot the energies of interest at ESRF, i.e. $-keV$. Figure 1.1 show the contribution for the attenuation coefficient, of the different absorption of a light material (water Figure 1.1a), and an heavi material (lead 1.1b) (from [SFV09]).

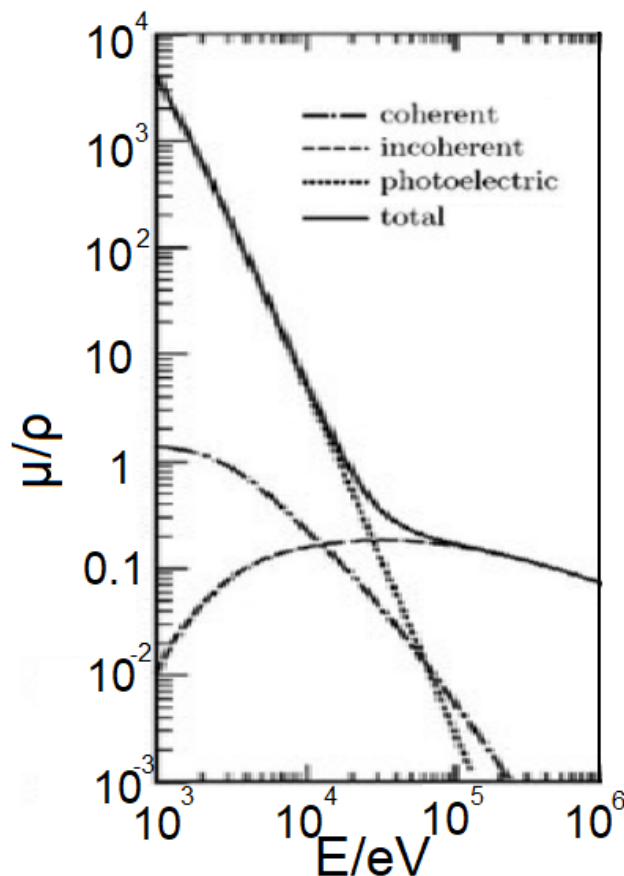
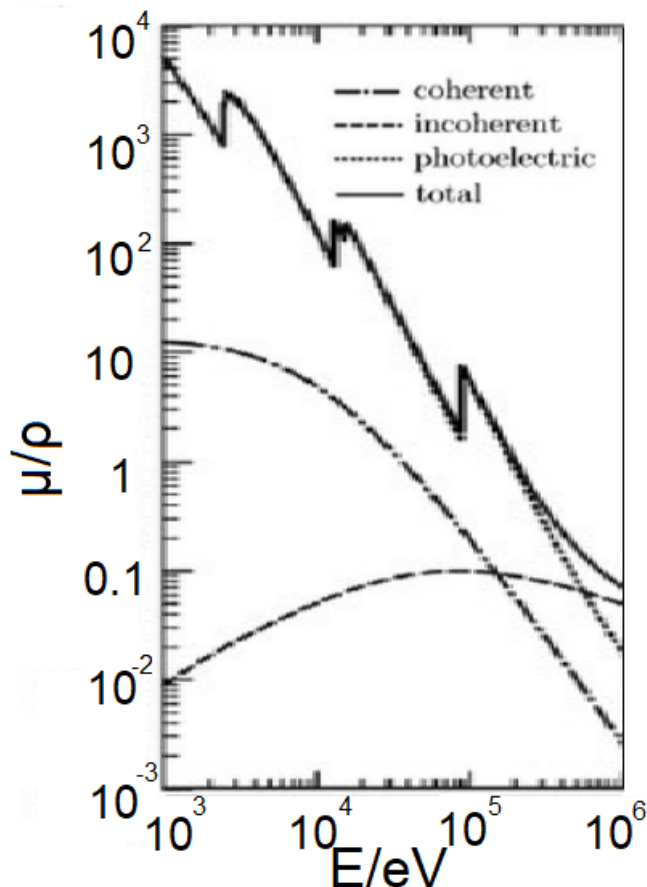
(a) H_2O (b) Pb

Figura 1.1: Attenuation coefficient for X-ray radiation of a light material (water Figure 1.1a), and an heavy material (lead 1.1b) (from [SFV09]).

1.1 Interaction with Matter

Interaction between radiation and matter can be compressed in an coefficient (absorption coefficient)), that rule the attenuation of an incident radiation

$$I = I_0 \exp(-\mu x) \quad (1.1)$$

where x is the thickness of the material, μ is the absorption coefficient, and I_0 the initial intensity of the beam corresponding to the intensity at $x = 0$. Considering the beam as a plane wave, it is possible to express the amplitude of the electromagnetic wave as:

$$A = A_0 \exp\left(\frac{-2\pi\beta x}{\lambda}\right) \exp\left(\frac{-2\pi i((1-\delta)x - ct)}{\lambda}\right) \quad (1.2)$$

where x is the position of the front wave, λ correspond to the wavelength of the wave in the vacuum, δ is a number that describe the dispersive aspect of the wave-matter interaction, and β is the absorption coefficient that describe the absorption aspect of the wave-matter interaction. The propagation of the radiation depend from the complex refractive index n , that can be expressed as:

$$n = 1 - \delta - i\beta \quad (1.3)$$

For X-rays process , the absorption term is the leading term, this mean that the μ coefficient can be defined as linearly dependent from the absorption coefficient, where:

$$\alpha = \frac{4\pi\beta}{\lambda} \quad (1.4)$$

Normally the absorption values tabulated are given are the mass absorption coefficients μ_m , where

$$\mu = \mu_m \rho \quad (1.5)$$

where ρ is the density of the material. The mass absorption of a compound is given by

$$\mu_{m,com} = \sum_j w_j \mu_{m,j} \quad (1.6)$$

where $\mu_{m,j}$ is the mass absorption of a particular element, and w_j is the fraction of the j element in the material. The relation between the absorption coefficient of the material and the mass absorption coefficient is:

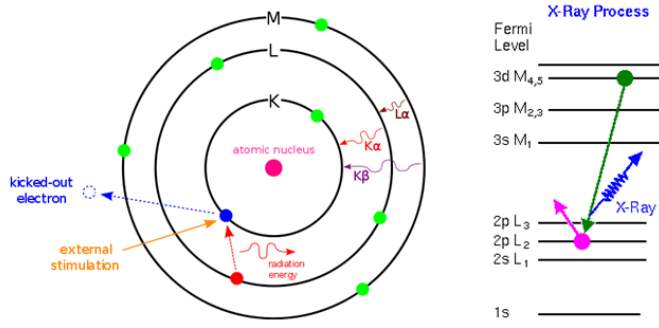


Figura 1.2: X-ray ionizing process

$$\alpha_{\text{com}} = \mu_{\text{m,com}} \rho_{\text{com}} \quad (1.7)$$

where ρ_{com} is the density of the compound.

Because of the dominant energy of the radiation with respect to the matter energies involved in the interaction (X-rays energies spreads from 100eV, soft X-ray, to 10keV, hard X-ray, binding and molecular energies are of the order of few eV), the ionization process, as said before, is the leading process in the absorption coefficient. In this case the greater part of the energies involved is transferred to the kinetic term of the ionized electrons. Electron in atom have a well-defined state of energies, so, to be absorbed, the radiation must have at least an energy equal to an electron state energies. For energies equal to the electron state energies, as showed in Figure 1.1, absorption edges appears. The nomenclature K, L, M , of those edges, that are not important for our treatment, correspond to, as it is showed in Figure 1.2, the energies of an electron that goes down from a greater level, for example $n = 2$ to a lower one $n = 1$ ([Aga91]). In reality, the edges, are less pronunciation as the ones in figure, due to the finite energy width of the states, and because of the environment effect.

To understand better the absorption of the X-ray radiation it is reported a brief theoretical treatment of the interaction, because the result are useful for the design of the optical element used for X-rays. The calculation start from the elastic scattering between X-ray photon against free electron (Thomson scattering). The electro-magnetic radiation is characterized by an electric field with amplitude A_0 that accelerate a free electron (of charge e and mass m_e) by an amount of $A_0(e/m)$. A charged particle that is accelerated emits radiation, this change the value of the amplitude of the electric field equal to:

$$A_T(\Phi) = \frac{e}{4\pi\varepsilon_0 c^2 \mathbf{r}} \mathbf{a} \sin \Phi \quad (1.8)$$

where r is the distance from the charge, Φ correspond to the angle between the position vector \mathbf{r} and acceleration vector \mathbf{a} . Replacing \mathbf{a} with $A_0(e/m)$:

$$A_T(\Phi) = A_0 \frac{e^2}{4\pi\varepsilon_0 c^2 \mathbf{r}} \sin \Phi \quad (1.9)$$

To treat the interaction between the bounded electron and the radiation, going beyond the Thomson scattering, it is possible to multiply the Thomson amplitude $A_T(\Phi)$ to a complex number is multiplied to a complex number $f = f_1 + if_2$ named complex atomic scattering. Thus:

$$A(\Phi, E) = A_t(\Phi) * f(E) = A_T(\Phi)[f_1(E) + if_2(E)] \quad (1.10)$$

where the two function f_1 and f_2 , depend on the energy of the incident X-ray radiation that, to a first approximation, are independent from the angle between the incident and the scattered radiation ϑ . This approximation has sense because the typical radiation length ($\sim 0.1 - 10\text{nm}$) is much larger than the typical length of the atomic electronic distribution ($\sim 1 - 50\text{pm}$), the consequence of this approximation is the possibility to consider a phase scattering of the atomic wave function. The values of the two function f_1 and f_2 are calculated in the relativistic quantum dispersion theory [CL70] and are given by:

$$f_1(E) = Z + 4\frac{\varepsilon_0 m_e c}{h e^2} \int_0^{+\infty} \frac{W^2 \sigma(W)}{E^2 - W^2} dW - \Delta_{rel} \quad (1.11)$$

and

$$f_2(E) = 2\frac{\varepsilon_0 m_e c}{h} E \sigma(E) \quad (1.12)$$

In Equation 1.11, the first term correspond to the Thomson scattering, where Z correspond to the atomic number of the atom. To add the angle-dependence of the scattering it is used the factor:

$$f_0 = \int_0^{+\infty} U(r) \operatorname{sinc} \left[\frac{4\pi r}{\lambda} \sin \frac{\vartheta}{2} \right] dr \quad (1.13)$$

where $U(r)$ represent the radial charge distribution and $\operatorname{sinc}(x)$ is the cardinal sine function $= \frac{\sin x}{x}$. Considering a wavelength λ of the order of nanometres, if $\sin \frac{\vartheta}{2} \leq \frac{\lambda}{2}$, $f_0 = Z$, otherwise for $\sin \frac{\vartheta}{2} = \lambda$, typically, for most element $f_0 \simeq 0.9Z$.

In Equation 1.11, the second term (the anomalous dispersion integral), represent the oscillation of the electron after the interaction with the radiation, this can be obtained treating the semi-classically the problem. This approach neglect the damping, so, near the absorption edges f_1 is inaccurate. The second term of the Equation 1.11, and in Equation 1.12 contain σ that is the photo ionization cross section expressed in $\text{m}^2 \text{atom}^{-1}$, a coefficient that is related to the mass absorption coefficient in this way:

$$\sigma(E) = A \frac{\mu}{N_0} \quad (1.14)$$

where A is the atomic weight and N_0 the Avogadro's number ($N_0 = 6.2210^{23} \text{ particlemol}^{-1}$). The value of $\sigma(E)$ is theoretically obtained knowing the atomic wave function of the atom, so, only for hydrogen it is possible to have the correct value, for all the other systems, the calculation can be done with approximation methods that give some uncertainty on $\sigma(E)$, consequently on the value of f_1 and f_2 .

In Equation 1.11 the third term takes into account the relativistic effect. This correction is given by [CL70]:

$$\Delta_{\text{rel}} = \frac{5}{3} \frac{|E_{\text{tot}}|}{m_e c^2} + \frac{Z}{2} \left(\frac{E}{m_e c^2} \right)^2 \quad (1.15)$$

where $|E_{\text{tot}}|$ is the modulus of the total energy of the atom (that is negative), moreover, this third term is the less relevant in Equation 1.11, for X-ray energies, so it is possible to neglect it in the calculation.

For photo absorption event by an electron bounded to an atom, far from the absorption edges, a good approximation is to consider the solid state environment distorted by the ionization of the electrons, because, the most affected electrons are the outer ones. After some calculation, it is possible to relate the factors f_1 and f_2 with the macroscopic parameters n and β :

$$\delta = 1 - n = \frac{e^2 \hbar^2}{2 \varepsilon_0 m_e E^2} \bar{f}_1 \quad (1.16)$$

and

$$\beta = \frac{e^2 \hbar^2}{2 \varepsilon_0 m_e E^2} \bar{f}_2 \quad (1.17)$$

where \bar{f}_1 and \bar{f}_2 are defined as follows:

$$\bar{f}_1 = \sum_j N_j f_{1j} \quad \bar{f}_2 = \sum_j N_j f_{2j} \quad (1.18)$$

and represent the average scattering factor per unit volume, N_j is the total number of the particular j element per unit volume. Putting everything together Equation 1.16, apart near the absorption edges, can be expressed as:

$$\delta = \frac{N e^2 \hbar^2}{2 \varepsilon_0 m_e E^2} \bar{f}_1 = \frac{N e^2 \lambda^2}{8 \pi^2 \varepsilon_0 m_e c^2} \bar{f}_1 \quad (1.19)$$

where N is the number of electrons per unit volume. For X-ray energies the value of δ is small (typically $\sim 10^{-3}$) and positive, this is important because it means that, for X-rays, the refractive index is a bit less than 1. It is possible to find the tabulated values of f_1 and f_2 , [?], that are the main ingredient to calculate the curve in Figure 1.1 and these were used to generate Figure 1. These values, according with the experimental results, allow to write, far from absorption edges, the absorption coefficient β such as:

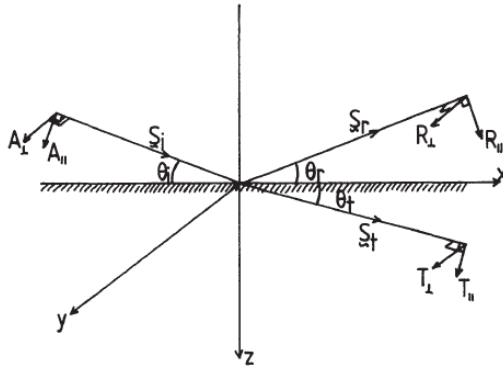


Figura 1.3: Interface of two medium

$$\beta \sim Z^2 \lambda^3 \quad (1.20)$$

This mean that increasing the photon energy, the absorption decrease, and it is consistent with Figure 1.1, far from the edges. Moreover, the absorption, become bigger with the element used in the optical element, heavy elements absorb more than light elements. This is the reason why, to use refractive lenses for x-ray radiation, one of the used material is the Beryllium.

1.2 Total External Reflection

For the system in Figure 3.15, there are two complex refractive index:

$$\bar{n}_1 = 1 - \delta_1 - i\beta_1 = n_1 - i\beta_1 \quad (1.21)$$

and

$$\bar{n}_2 = 1 - \delta_2 - i\beta_2 = n_2 - i\beta_2 \quad (1.22)$$

moreover $\delta_2 > \delta_1$. In the general case there are, as shown in Figure 3.15 a reflected and a transmitted wave. For the theoretical treatment, initially, will be neglect the absorption ($\beta_1 = \beta_2 = 0$), moreover the permeability coefficient it is supposed to be similar to the permeability in the vacuum. Thus, the law of Snell, can be expressed such as:

$$\frac{\cos \vartheta_i}{\cos \vartheta_t} = \frac{1 - \delta_2}{1 - \delta_1} \quad (1.23)$$

Using the frame system as in Figure 3.15, with the z-axis that correspond to the normal of the interface. It is possible to write the component of the electric field of the waves in this way

$$E_{ix} = A_{\parallel} \sin \vartheta_i \exp^{-i\tau_i}, \quad E_{iy} = A_{\perp} \exp^{-i\tau_i}, \quad E_{iz} = A_{\parallel} \cos \vartheta_i \exp^{-i\tau_i} \quad (1.24a)$$

$$E_{tx} = -T_{\parallel} \sin \vartheta_t \exp^{-i\tau_t}, \quad E_{ty} = T_{\perp} \exp^{-i\tau_t}, \quad E_{tz} = T_{\parallel} \cos \vartheta_t \exp^{-i\tau_t} \quad (1.24b)$$

$$E_{rx} = R_{\parallel} \sin \vartheta_r \exp^{-i\tau_r}, \quad E_{ry} = R_{\perp} \exp^{-i\tau_r}, \quad E_{rz} = R_{\parallel} \cos \vartheta_r \exp^{-i\tau_r} \quad (1.24c)$$

where

$$\tau_i = \omega(t - \frac{\mathbf{r} \bullet \mathbf{s}_i}{v_1}) = \omega \left[t - \frac{(1 - \delta_1)(x \cos \vartheta_i + z \sin \vartheta_i)}{c} \right] \quad (1.25a)$$

$$\tau_t = \omega(t - \frac{\mathbf{r} \bullet \mathbf{s}_t}{v_2}) = \omega \left[t - \frac{(1 - \delta_2)(x \cos \vartheta_t + z \sin \vartheta_t)}{c} \right] \quad (1.25b)$$

$$\tau_r = \omega(t - \frac{\mathbf{r} \bullet \mathbf{s}_r}{v_1}) = \omega \left[t - \frac{(1 - \delta_1)(x \cos \vartheta_r + z \sin \vartheta_r)}{c} \right] \quad (1.25c)$$

where ω is the angular frequency of the wave, and v_1, v_2 , correspond to the velocities of propagation that depend on the material as follow:

$$v_1 = \frac{c}{1 - \delta_1}, \quad v_2 = \frac{c}{1 - \delta_2} \quad (1.26)$$

the related magnetic field are:

$$\begin{aligned} H_{ix} &= -A_{\perp}(1 - \delta_1) \sin \vartheta_i \exp^{-i\tau_i}, & H_{iy} &= -A_{\parallel}(1 - \delta_1) \exp^{-i\tau_i}, \\ H_{iz} &= A_{\perp}(1 - \delta_1) \cos \vartheta_i \exp^{-i\tau_i} \end{aligned} \quad (1.27a)$$

$$\begin{aligned} H_{tx} &= -T_{\perp}(1 - \delta_2) \sin \vartheta_t \exp^{-i\tau_t}, & H_{ty} &= -T_{\parallel}(1 - \delta_2) \exp^{-i\tau_t}, \\ H_{tz} &= T_{\perp}(1 - \delta_2) \cos \vartheta_t \exp^{-i\tau_t} \end{aligned} \quad (1.27b)$$

$$\begin{aligned} H_{rx} &= -R_{\perp}(1 - \delta_1) \sin \vartheta_r \exp^{-i\tau_r}, & H_{ry} &= -R_{\parallel}(1 - \delta_1) \exp^{-i\tau_r}, \\ H_{rz} &= R_{\perp}(1 - \delta_1) \cos \vartheta_r \exp^{-i\tau_r} \end{aligned} \quad (1.27c)$$

the boundary condition impose the continuity of the fields:

$$E_{ix} + E_{rx} = E_{tx}, \quad E_{iy} + E_{ry} = E_{ty} \quad (1.28)$$

and

$$H_{ix} + H_{rx} = H_{tx}, \quad H_{iy} + H_{ry} = H_{ty} \quad (1.29)$$

because of Snell's laws $\vartheta_r = \vartheta_t$, so, from the Equation 1.28 and Equation 1.29:

$$(A_{\parallel} - R_{\parallel}) \sin \vartheta_i = T_{\parallel} \sin_t \quad (1.30a)$$

$$A_{\perp} + R_{\perp} = T_{\perp} \quad (1.30b)$$

$$(1 - \delta_1)(A_{\perp} - R_{\perp}) \sin \vartheta_i = (1 - \delta_2)T_{\perp} \sin \vartheta_t \quad (1.30c)$$

$$(1 - \delta_1)(A_{\parallel} + R_{\parallel}) = (1 - \delta_2)T_{\parallel} \quad (1.30d)$$

Equations 1.30 give a set of equations where the parallel and perpendicular component of the waves are independent. Solving that set with respect to each parallel/perpendicular component it is obtained:

$$\frac{R_{\parallel}}{A_{\parallel}} = \left[\frac{(1 - \delta_2) \sin \vartheta_i - (1 - \delta_1) \sin \vartheta_t}{(1 - \delta_2) \sin \vartheta_i} + (1 - \delta_1) \sin \vartheta_t \right] \quad (1.31a)$$

$$\frac{R_{\perp}}{A_{\perp}} = \left[\frac{(1 - \delta_1) \sin \vartheta_i - (1 - \delta_2) \sin \vartheta_t}{(1 - \delta_1) \sin \vartheta_i} + (1 - \delta_2) \sin \vartheta_t \right] \quad (1.31b)$$

$$\frac{T_{\parallel}}{A_{\parallel}} = \frac{2(1 - \delta_1) \sin \vartheta_i}{(1 - \delta_2) \sin \vartheta_i + (1 - \delta_1) \sin \vartheta_t} \quad (1.31c)$$

$$\frac{T_{\perp}}{A_{\perp}} = \frac{2(1 - \delta_1) \sin \vartheta_i}{(1 - \delta_1) \sin \vartheta_i + (1 - \delta_2) \sin \vartheta_t} \quad (1.31d)$$

Equations 1.31 are the **Fresnel formula** for reflection at a plane surface. Combining them with Equation 1.23 it is obtained:

$$\frac{R_{\parallel}}{A_{\parallel}} = \frac{(1 - \delta_2)^2 \sin \vartheta_i - (1 - \delta_1) \sqrt{(1 - \delta_2)^2 - (1 - \delta_1)^2 \cos^2 \vartheta_i}}{(1 - \delta_2)^2 \sin \vartheta_i + (1 - \delta_1) \sqrt{(1 - \delta_2)^2 - (1 - \delta_1)^2 \cos^2 \vartheta_i}} \quad (1.32a)$$

$$\frac{R_{\perp}}{A_{\perp}} = \frac{(1 - \delta_1)^2 \sin \vartheta_i - \sqrt{(1 - \delta_2)^2 - (1 - \delta_1)^2 \cos^2 \vartheta_i}}{(1 - \delta_1)^2 \sin \vartheta_i + \sqrt{(1 - \delta_2)^2 - (1 - \delta_1)^2 \cos^2 \vartheta_i}} \quad (1.32b)$$

$$\frac{T_{\parallel}}{A_{\parallel}} = \frac{2(1 - \delta_1)(1 - \delta_2) \sin \vartheta_i}{(1 - \delta_2)^2 \sin \vartheta_i + (1 - \delta_2) \sqrt{(1 - \delta_2)^2 - (1 - \delta_1)^2 \cos^2 \vartheta_i}} \quad (1.32c)$$

$$\frac{T_{\perp}}{A_{\perp}} = \frac{2(1 - \delta_1) \sin \vartheta_i}{(1 - \delta_1) \sin \vartheta_i + \sqrt{(1 - \delta_2)^2 - (1 - \delta_1)^2 \cos^2 \vartheta_i}} \quad (1.32d)$$

When ϑ_i is such that:

$$\cos \vartheta_c = \frac{1 - \delta_2}{1 - \delta_1} \quad (1.33)$$

that angle is named critical angle ϑ_c , and

$$\frac{R_{\parallel}}{A_{\parallel}} = \frac{R_{\perp}}{A_{\perp}} \quad (1.34)$$

this case correspond to a wave that is totally reflected. Normally the total external reflection take place at an interface light material(air/vacuum) and dense material, so $\delta_1 = 0, \delta_2 = \delta$, the equations became:

$$\cos \vartheta_c = 1 - \delta \quad \text{for small angle} \quad \vartheta_c \simeq \sqrt{2\delta} \quad (1.35)$$

and:

$$\frac{R_{\parallel}}{A_{\parallel}} = \frac{(1-\delta)^2 \sin \vartheta_i - \sqrt{(1-\delta)^2 - \cos^2 \vartheta_i}}{(1-\delta)^2 \sin \vartheta_i + \sqrt{(1-\delta_2)^2 - \cos^2 \vartheta_i}} \quad (1.36a)$$

$$\frac{R_{\perp}}{A_{\perp}} = \frac{\sin \vartheta_i - \sqrt{(1-\delta)^2 - (1-\cos^2 \vartheta_i)}}{\sin \vartheta_i + \sqrt{(1-\delta)^2 - \cos^2 \vartheta_i}} \quad (1.36b)$$

$$\frac{T_{\parallel}}{A_{\parallel}} = \frac{2(1-\delta) \sin \vartheta_i}{(1-\delta)^2 \sin \vartheta_i + \sqrt{(1-\delta)^2 - (1-\cos^2 \vartheta_i)}} \quad (1.36c)$$

$$\frac{T_{\perp}}{A_{\perp}} = \frac{2 \sin \vartheta_i}{\sin \vartheta_i + \sqrt{(1-\delta)^2 - \cos^2 \vartheta_i}} \quad (1.36d)$$

introducing the absorbing coefficient $\beta_2 = \beta \neq 0$:

$$\frac{R_{\parallel}}{A_{\parallel}} = \frac{\bar{n}^2 \sin \vartheta_i - \sqrt{\bar{n}^2 - \cos^2 \vartheta_i}}{\bar{n}^2 \sin \vartheta_i + \sqrt{\bar{n}^2 - \cos^2 \vartheta_i}} \quad (1.37a)$$

$$\frac{R_{\perp}}{A_{\perp}} = \frac{\sin \vartheta_i - \sqrt{\bar{n}^2 - \cos^2 \vartheta_i}}{(\sin \vartheta_i + \sqrt{\bar{n}^2 - \cos^2 \vartheta_i})} \quad (1.37b)$$

$$\frac{T_{\parallel}}{A_{\parallel}} = \frac{2\bar{n} \sin \vartheta_i}{\bar{n}^2 \sin \vartheta_i + \sqrt{\bar{n}^2 - \cos^2 \vartheta_i}} \quad (1.37c)$$

$$\frac{T_{\perp}}{A_{\perp}} = \frac{2 \sin \vartheta_i}{\sin \vartheta_i + \sqrt{\bar{n}^2 - \cos^2 \vartheta_i}} \quad (1.37d)$$

For interface that are curved, the Equations 1.37 are still valid if the curvature radius is much grater than the wavelength, condition that is satisfied for the X-ray radiation. The reflectivity are defined in these way::

$$R_p = \frac{R_{\parallel}}{A_{\parallel}} \left(\frac{R_{\parallel}}{A_{\parallel}} \right)^* \quad (1.38)$$

and

$$R_p = \frac{R_{\parallel}}{A_{\parallel}} \left(\frac{R_{\parallel}}{A_{\parallel}} \right)^* \quad (1.39)$$

Figure 1.4, show the behaviour of an ideal non absorbing material ($\beta = 0$), where the reflection maintain its initial value up to the critical angle, and after fall down, in a way ruled by the dispersion coefficient δ which depend on the energy. In reality β is never zero, so it is not possible to have total external reflection in the way defined before. It is convenient to define that the total external appear when there is a point of inflection in the reflection curve with respect to the incidence angle ϑ_i , this occurs when:

$$\beta < 0.63\delta \quad (1.40)$$

In Figure 1.5 are plotted the reflectivity trend of three material (Si, Rh, Pb) with respect to the incidence angle, fixing the energy of the radiation at 5000eV, on a silicon substrate. As it is figured there is a better behaviour, in sense of critical angle, for the light element because of them minor absorption coefficient β . This dependant mirror reflectivity is not implemented in my python library MONWES (but it could be done).

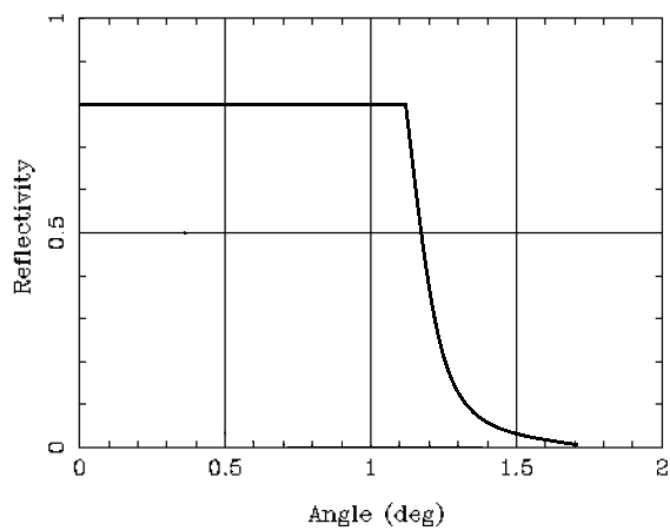


Figura 1.4: Reflectivity for the case of a non-absorbing material

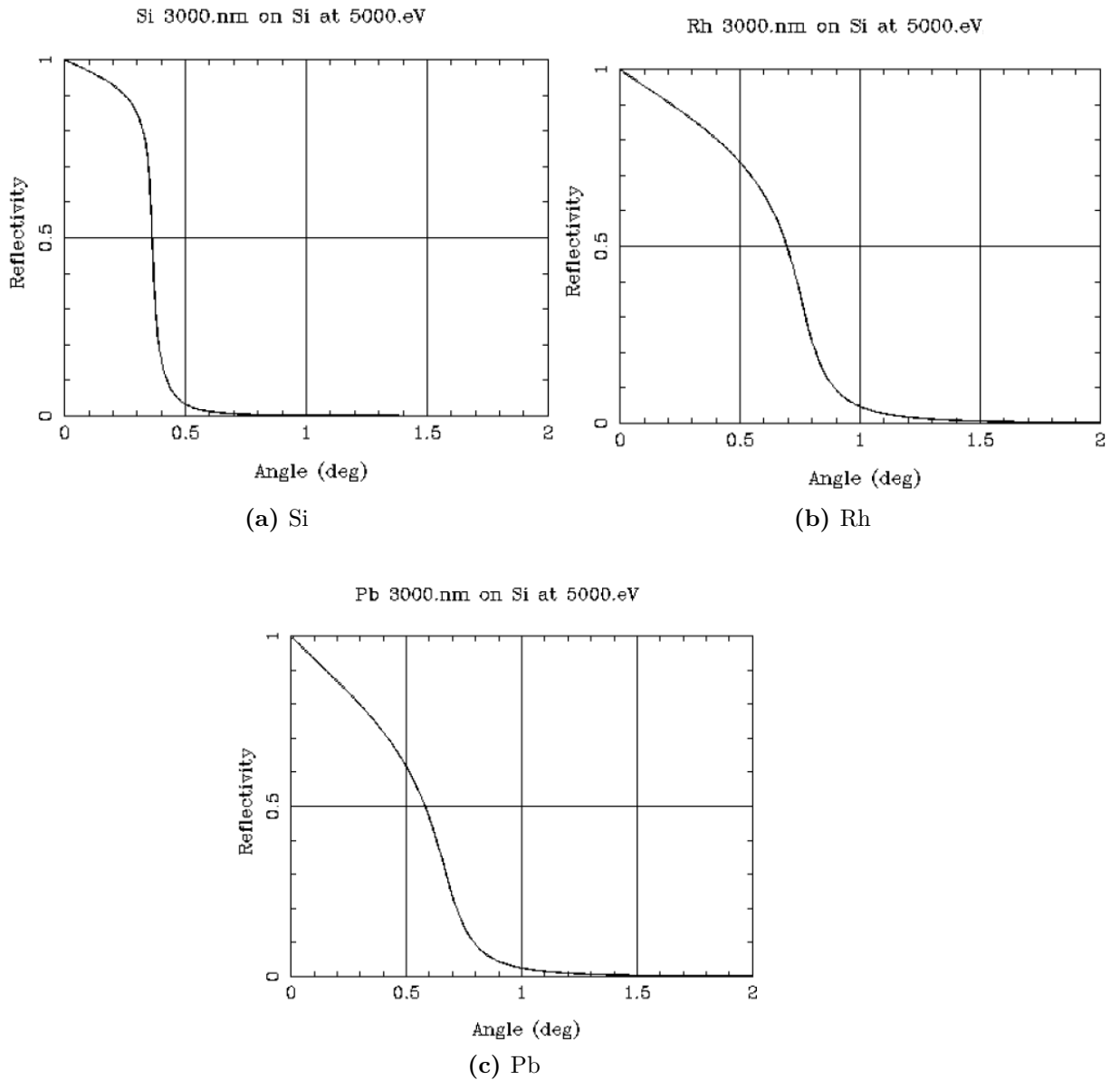


Figura 1.5: Reflectivity plot with respect of the grazing incidence angle ϑ_i of different material with a radiation of 500eV on a substrate of Si [LBN10]

Capitolo 2

Mirrors for X-rays

As discussed in Chapter 1, to focus X-ray radiation, it can be used refraction (compound refractive lenses) and reflection optics (curved mirrors). In this chapter will be discussed the reflection optics because they are the main elements used in my python library. These optics are used in a grazing configuration because of their values of small critical angle for the total external reflection for X-ray radiation. The first part of this Chapter discuss the focusing property of the simplest curved mirror, spherical one, showing that it can't be used due to its intrinsic aberration that are huge in a grazing incidence configuration. After will be introduced the toroidal and conical mirror, that cancel out some kind of aberration with respect to the spherical mirror. In the last part are discussed the concept of imaging system, thus is explained two configuration of conical mirror used to focus the radiation in the synchrotron beamline. The KirckPatrick-Baez system, very popular at ESRF, and the Montel system, that is the main object of my thesis.

2.1 Spherical surface

Mirrors that carry out any focusing must have a curved surface, and the simplest one, that it is defined only by one parameter, the radius of curvature, is the spherical mirror. This mirror work well for normal incidence reflection, but, in a grazing configuration, its affected by many kind of aberration. Here are discussed the:

1. astigmatism
2. spherical aberration

that are the main aberration that affect X-ray radiation.

2.1.1 Astigmatism

Astigmatism is the effect that focus a ray, which propagate in two perpendicular planes, in different point. In Figure 2.1 it is showed an image formation of a beam with a spherical mirror of radius R , at grazing incidence ϑ_i . Supposing that all the rays exiting from the source P are focused in the same point Q, and considering only the part of the beam that hit the portion of the mirror NO, it is possible to

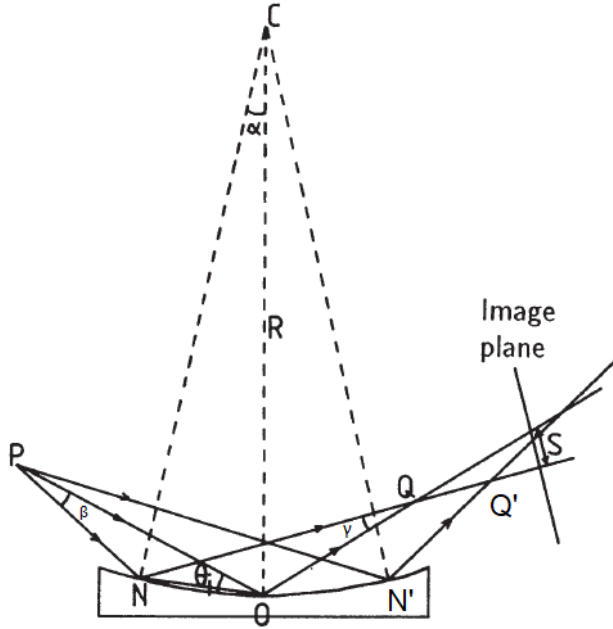


Figura 2.1: Formation image of a circular mirror for a point-wise source placed at a distance PO from the center of the mirror. R is the curvature of the mirror, ϑ_i the angle of the central ray.

define β as the source divergence, γ the image divergence, u the distance PO and v the distance OQ . The beam hit the mirror over a distance equal to $k = NO$, such as $k \ll R$, that correspond to a small divergence β . The cord NO subtends an angle α with the center of the sphere C , thus $k = R\alpha$, γ is the convergence angle of the beam at the focal point Q . For small angle approximation, from the triangle PNO ,

$$\beta = R\alpha \frac{\vartheta_i - \alpha/2}{u - R\alpha} \quad (2.1)$$

and from QNO

$$\gamma = R\alpha \frac{\vartheta_i + \alpha/2}{v + R\alpha} \quad (2.2)$$

The reflection law impose that $\beta + \gamma = 2\alpha$, thus:

$$\frac{1 - \alpha/(2\vartheta_i)}{u - R\alpha} + \frac{1 + \alpha/(2\vartheta_i)}{v + R\alpha} = \frac{2}{R\vartheta_i} \quad (2.3)$$

in case of paraxial approximation

$$\frac{1}{u} + \frac{1}{v} = \frac{2}{R\vartheta_i} = \frac{1}{f_m} \quad (2.4)$$

where

$$f_m = \frac{R\vartheta_i}{2} \quad (2.5)$$

more generally

$$f_m = \frac{R \sin \vartheta_i}{2} \quad (2.6)$$

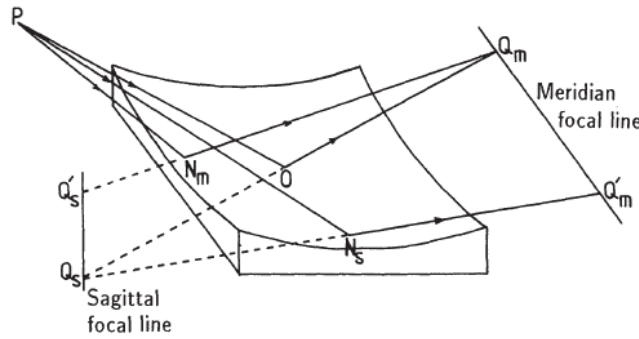


Figura 2.2: Image formation of a spherical mirror. The formation of a point wise source correspond to a two rods, one in the sagittal plane, and the second one in the meridial plane

f_m is named meridian focal length.

In case of a spherical mirror, a second image is generated in the sagittal plane, as it is showed if Figure 2.2, with a focal distance equal to:

$$f_s = \frac{R}{2 \sin \vartheta_i} \quad (2.7)$$

and it is named sagittal focal length. For Figure 2.2 it is possible to note that the two image for a point wise source are lines, where the meridial line is in the plane of the mirror and the sagittal line perpendicular to it. Equation 2.5 and Equation 2.7, are equal for incidence angle $\vartheta_i = 90^\circ$, and correspond to have a stigmatic image (image without astigmatism). In the case of grazing incidence the situation is bad, for example, with a $\vartheta_i = 2^\circ$, the sagittal focal length is 10^3 times the meridial length.

2.1.2 Spherical Aberration

Another aberration that affected a spherical mirror is the one named spherical aberration. Figure 2.1 show that the ray are focused in different position, depending on the portion of the mirror that hit, for example the ray PN is focused in Q , and the ray PN' in Q' . This aberration can be determined relating it with the variation of v with α :

$$S = \Delta v \sin \gamma \simeq \Delta v \gamma \quad (2.8)$$

where S is the image size that determine the spherical aberration. Moreover, from Equation 2.3, in case of $\alpha = 0$:

$$v_0 = \frac{f_m u}{u - f} \quad (2.9)$$

otherwise:

$$v = v_0 + \Delta v = f_m u - \frac{\frac{3uR\alpha}{4} + \frac{R^2\alpha^2}{2}}{u - \frac{3R\alpha}{4} - f_m} \quad (2.10)$$

defining a magnification such as

$$M = \frac{v}{u} \quad (2.11)$$

combining it with Equation 2.1 and Equation 2.2

$$\gamma = \frac{2\alpha}{M+1} \quad (2.12)$$

So

$$S = \frac{3R\alpha^2}{2}(M+1) = \frac{3k^2}{2R}(M+1) \quad (2.13)$$

the dependence of S with respect to k is quadratic, so all the rays are deviated to the same side of $\alpha = 0$ image point.

2.1.3 Reducing aberration

For spherical mirror it is possible to reduce the aberration using large grazing angle (decrease astigmatism) and small aperture (decrease spherical aberration). The first solution is limited by the ϑ_c , for the total external reflection of the order of some milliradian, for X-ray energies, that create a very huge astigmatism for spherical mirror. Reducing the aperture it means to reduce k but, this, affect the collecting power of the mirror reducing it. This is bad because the resolving power is limited by the diffraction limit that is $\simeq \frac{\lambda}{2\vartheta}$, where ϑ is the maximum semiaperature, that, for grazing angle, correspond to ϑ_i .

There is another way to reduce or cancel the aberration, using mirrors with different shape. If it want to reduce the astigmatism, toroidal mirror are very useful, if it want to reduce spherical aberration ellipsoidal mirror can be used used. These kind of aspherical mirror are reported in the following section.

2.2 Conic Surfaces

As said before, to go beyond the spherical mirror correcting the aberration, there exist aspherical surfaces that are defined with more than one parameter, in general by an analytical formula. The easier aspherical surface is the toroidal surface, a surface that is defined with two radii of curvature, the meridian one R_m and the sagittal one R_s . A particular choice of radii can be

$$R_m \sin \vartheta_i = \frac{R_s}{\sin \vartheta_i} \quad (2.14)$$

in such a way to have equal focal length and so no astigmatism. Thus

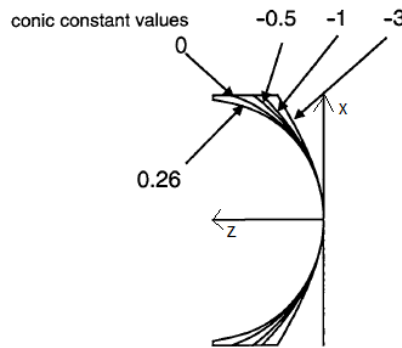
$$R_s = R_m \sin^2 \vartheta_i \quad (2.15)$$

Other kind of aspherical surfaces are those named "conic surfaces" that can be defined, approximately, as

$$z = \frac{cx^2}{1 + \sqrt{1 - (1+k)c^2x^2}} \quad (2.16)$$

where c is the base curvature at the vertex, k is a constant that define the kind of conical surface, and x is the radial coordinate of the point on the surface. In Table

Conic Constant k	Surface Type
0	Circle
$k < -1$	Hyperbola
$k = -1$	Parabola
$-1 < k < -0$	Ellipse
$k > 0$	Oblate Ellipse

Tabella 2.1: Parameter of different conic surfaces**Figura 2.3:** Different kind of surface conic, with the same c base curvature value, and different constant k .

2.1, and in Figure 2.3 is showed the relation between the k constant and the kind of surface

A good point that have the conical surfaces are the no-presence of spherical aberration. As said in before, spherical surface affected buy spherical aberration if the configuration is away from the normal incidence. The ellipsoidal geometry forms create a free-aberration image for a couple of real object on the same side of the surface, on the contrary the hyperbola work for conjugates on different side of it. Parabolic surface create a perfect image for any axial object place at infinity, this is the reason why parabolic mirror are very used for astronomical application. For all the shapes of surfaces, if the object is moved from it's ideal position aberration will appear: an axial movement introduce a certain amount of spherical aberration, lateral movement introduce other types of aberration such as coma, astigmatism and field curvature.

Figure 2.4 show a simple example of how it is possible to correct the spherical aberration using a paraboloid mirror 2.4b instead of a spherical mirror 2.4a

2.3 Compound Optical system

Simple mirror work well for a point to point optical system, but, to reproduce correctly an object image with the same aspect ratio it needed an imaging system. A system like this must satisfy the Sine-Abbe condition

$$\frac{\sin u'}{\sin U'} = \frac{\sin u}{\sin U} \quad (2.17)$$

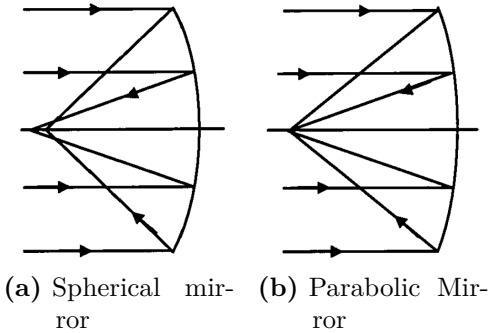


Figura 2.4: Example of spherical aberration correction

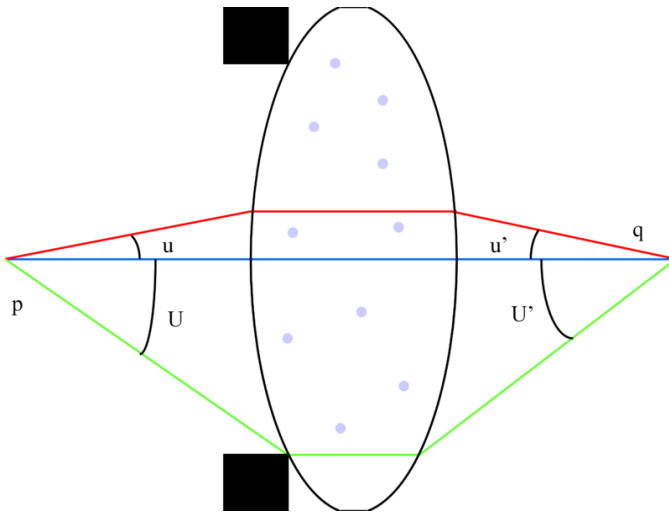
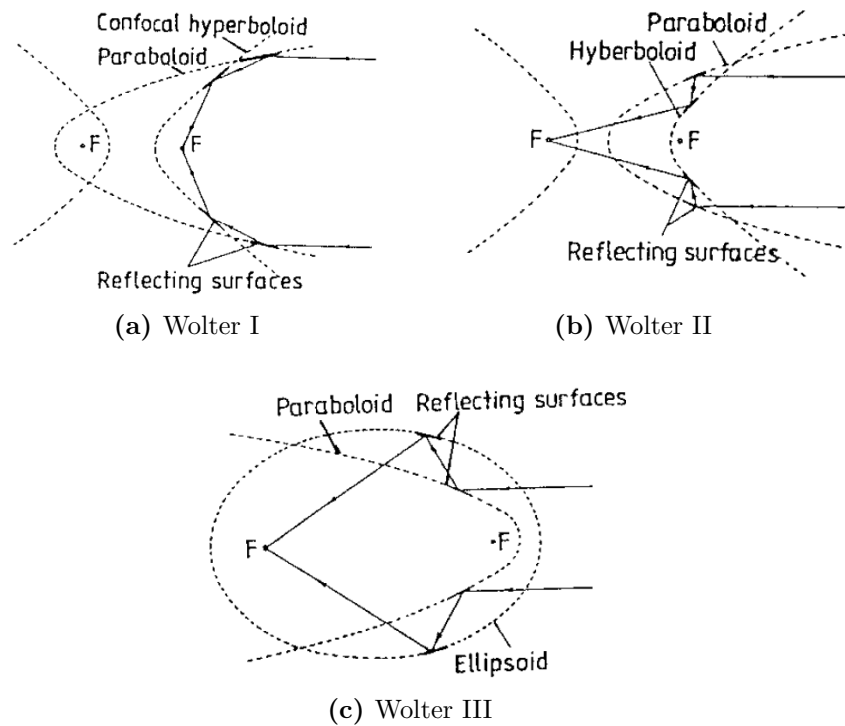


Figura 2.5: Sine Abbe condition for a lens

where, as it is showed in Figure 2.5, u and u' are rays that leave the object, U and U' are the angles of the same rays that reach the image plane. In other world, the sine of the ray that leave the object must be proportional to the sine of the angles that reach the image plane. Unfortunately, for the case of mirror, there is no way to satisfy the Sine Abbe condition using only one mirror. To satisfy the condition, and so obtain a better image, there are optical system composed by more than one mirror. The system that whose invented which respect the condition are the Wolter system, widely used in astronomy, that use a combination of coaxial and confocal conic section. A first approximation system that respect the sine Abbe condition are the Kirkpatrick-Baez system and Montel or nested-Kirkpatrick-Baez system, those compound optical system involves reflector whose meridian planes are at right angle (crossed).

2.3.1 Wolter System [SS05]

In 1952 Wolter published a paper in which he discussed several disposition of two conical mirror in order to collect light for an astronomical use. Figure show the different disposition discussed: Wolter I, Wolter II, Wolter III. Wolter I telescope consist of a coaxialparaboloid (primary mirror) and hyperboloid (secondary mirror).



The focus of the paraboloid is coincident with the rear focus of the hyperboloid, and the reflection inside both mirrors. The Wolter II telescope use the same kind of mirror of Wolter I paraboloid and hyperboloid. But the focus of the paraboloid coincident with the front focus of the hyperboloid, and, the reflection, occurs internally for the paraboloid and externally for the hyperboloid. The Wolter III telescope consist in a paraboloid and an ellipse. In this system the first mirror is the paraboloid one, and the second is the ellipsoidal that have front focus coincident with that of the parabola, moreover the reflection is external for the paraboloid and internal for the ellipsoidal. The Wolter I have typical grazing angle of less than a degree and is used for hard X-rays. The Wolter II telescope has typical grazing angle of, approximate, 10 degree and is used for soft X rays and extreme ultraviolet (EUV). Because of circular symmetry, astigmatism and spherical aberration are eliminated but exhibit coma aberration. Other problem is the difficulty of fabrication , and require a huge area to achieve a very small collecting angle.

2.3.2 Kirkpatrick-Baez System [MY09]

In 1948, Kirkpatrick and Baez proposed an X-ray focusing optical system consisting of two total reflection elliptical mirrors, which aligned perpendicularly (Figure 2.6). This focusing optical system is very popular at the ESRF due to its potential to remarkably improve the performance characteristics of X-ray microscopy by enabling more efficient collecting of X-rays than in other methods. A further advantage is that the method maintains the focusing state with the same optical arrangement even if the wavelength of the X-rays is shifted. However, to realize X-ray beams with an ideal focal size, high efficiency and absence of background

noise around a main peak, it is necessary to prepare elliptical mirrors having a very high quality. Since the two mirrors are not coincident, the object distance for the meridian reflection in the first mirror is less than that for the sagittal reflection in the second mirror. Thus the magnification is different in the two direction.

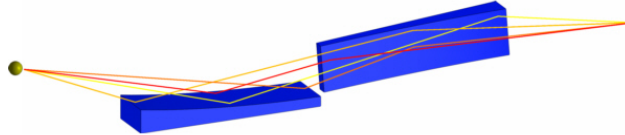


Figura 2.6: Kirkpatrick-Baez system

2.4 Montel

Another possibilities to dispose mirrors creating a focalizing or colimating optical system consist in the disposition of two orthogonal mirror attached one to the other as showed in Figure 2.7. This geometry is called Nested Kirkpatrick-Baez system or Montel system [Mon57]. Up to know were described element well-known and well-studied in the state of art. To go beyond current performance however, new approaches are required that can collect more divergence than with standard sequential Kirkpatrick-Baez (KB) X-ray mirrors and that can collect the greatest possible intensity into small beams for neutron optics. Indeed, the quality of x-ray mirrors has now reached the diffraction limit, and simply more perfect KB mirrors cannot decrease spot size.

In this section is done a first description of the Montel system with its advantages and disadvantages with respect to the KB system. After there is an explanation on the designing method of Montel system.

2.4.1 Description

Because of its distinctive design, Montel system have numerous advantages over traditional Kirkpatrick–Baez system. In contrast to KB systems where the two reflective surfaces are arranged in-line one after the other, those in Montel optics are mounted side by side at 90 to each other (Figure 2.7). Due to this fact, the incident X-ray beam now undergoes reflection simultaneously from both surfaces instead of being reflected sequentially as in the KB system. Hence, the mirror-focal point distance is diminished and consequently the demagnification ratio increased. The gain can be substantial especially when the focal distance is comparable with the mirror lengths. Furthermore, the side-by-side geometry offers a more compact design and therefore represents a convenient solution when space availabilities for optical elements are highly restrictive. In terms of mechanical structures, KB optics usually require two independent sets of alignment stages for each mirror. It is possible, in the Montel system, to assemble both surfaces together with their stages onto a common platform. Apart from providing a compact solution, this can also help in reducing the sources of parasitic vibrations as well as any individual misalignment between the mirrors. Lastly, since in this geometry that want to the

second mirror is positioned closer to the source than in the KB system, for the same angular acceptance in both mirror systems, a shorter mirror is needed in the Montel optics design. This is highly desirable as significantly better figure errors can be achieved for smaller mirror sizes than larger ones with the overall benefit of yielding less aberrated beams.

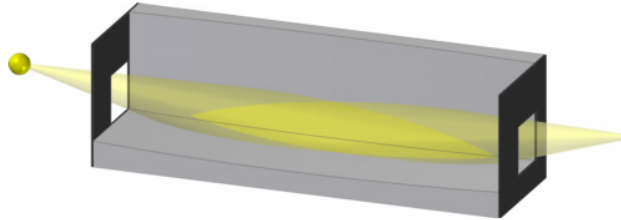


Figura 2.7: Montel system

On the other, the Montel configuration, present some draw-back with respect to the sequential KB system. A first on is due to the fact that the beam hit the worst part of the mirrors, the edge, that are less polished part containing a great part of surface defect.

2.4.2 Optical Design [IBK09]

The mirrors used in this Montel configuration are mirror that have a cylindrical shape in one direction and elliptical shape in the other direction. One approach to obtain the Montel system is that to use two pre-figured elliptical mirror and grind the cut site at 45° as shown in figure. After that it place the mirrors together makes a good fit with no gap requiring no contouring of the mirror side. Another way involves diving pre-figured elliptical mirror into two part that, add them together, can form the Montel system. This approaches is primary driven by the fact that in a conventionally polished mirror, the clear aperture area has the best figure and finish. As such, using two halves of a prefigured mirror cut in the middle has several advantages- including consistency and economy. There are major challenges however. First, the mirror surface must be protected against damage and deformation during cutting and subsequent figuring operations. After cutting into two, the cut sites must be treated (e.g., etched) to remove any subsurface damages that could alter a mirror's figure. Then the mating side of one of the mirrors must be contoured and polished such that when it is placed against the partner mirror, it makes a nearly perfect fit with good surface quality all the way to the contact edge. This last two-steps are crucial because if there is a significant gap or if the mirror surfaces in the vicinity of the interface are damaged, a significant part of the incident beam could be lost. As an example, we are developing a pair of Montel mirrors for poly chromatic nanofocusing on Sector 33 at APS. This beam line will use 40 mm long elliptical mirrors for nano-focusing a $100 \mu\text{m}$ beam to a 50 nm spot at 2000x demagnification. This concave elliptical mirror has a maximum depression of about $6 \mu\text{m}$ at its center. If cut flat and placed against its mating mirror, a gap as large as $6 \mu\text{m}$ is created which loses about 10% of the $100 \mu\text{m}$ incident beam. Similarly,

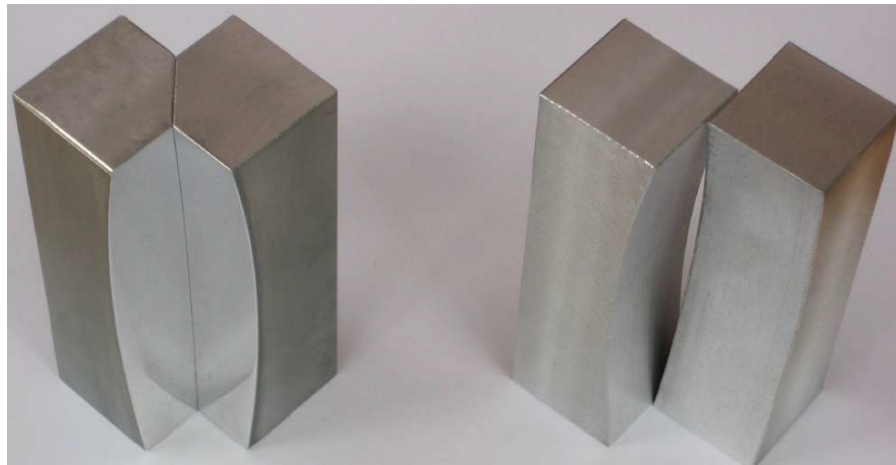


Figura 2.8: Example in how to build a Montel system starting from two cylindrical mirror cutting the edge with ad angle of 45° .

if the mirror surfaces near the intersection are damaged, then beam loss can be significant.

Capitolo 3

MONWES

Chapter 3 goes deep in the description of the python library developed by me. Monwes (MOntel and Wolter of yunES) library is a python library that perform ray tracing simulations for x-ray radiation along a system consisting of one or several mirror, using the optical element and compound optical elements introduced in Chapter 2 (MONWES is still on working, the implementation of Wolter systems are not been done yet). The library take inspiration from OASYS ray tracing software developped by Manuel Sanchez Del Rio of ESRF, taking the starting element already present in OASYS environment in order to have the basic element that will be used in the new Montel system. OASYS elements are written for a sequential tracing method, method that doesn't work for Montel system. Thus a great effort has been done to generate a new tracing system that use a parallel approach.

Object oriented programming were used consisting in a programming method in which data structures are defined with their type of operation, that are applied to the data structure. This oriented programming is based on the concept of "objects", it contain data in form of fields known as attributes and code in the form of procedure known as methods [GHJV95].

The final goal of the MONWES library is that to complement the standatd ray tracing code SHADOW in OASYS with compound elements.

The library, and so this Chapter, is composed by three main element:

1. Beam object: containing the information of the beam along the beamline;
2. Optical element: that initialize the characteristic of the optical element/system used in the beamline;
3. Tracing system: that related the Beam characteristic with the effect of the optical elements/systems.

3.1 Beam

Beam object is the object that contain the spatial and velocity information of a collection of rays. The Beam object is mainly characterized by four parameters:

- Number of rays
- Spatial profile
- Divergence profile
- Flag vector

Having a large number of rays is useful in terms of results but, as a back draw, increase the computation time, so, it have to find a compromise between the number of rays and the computation time depending on the quality desired. By default, the number of rays, is set $25 * 10^3$ that allow to have good results without spending lot of time. Figure 3.1 show an initialization of Beam setting the number of ray equal to 10^4 .

```

1  from monwes.Beam import Beam
2
3  beam = Beam(N=10**4)

```

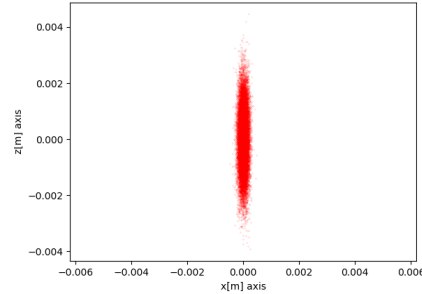
Figura 3.1: Example of Beam initialization

Defined the Beam with its number of rays it have to choose the spatial and divergence profile. For the spatial profile there are some possibilities that correspond to different geometrical figure such as: rectangular profile, circular profile, Gaussian profile, point wise profile. The default one is the point wise profile, that it is useful for ideal testing, obviously, for this case, there is no input parameter. All the other profile are characterized by external input in order to define the profile depending on the nature of the profile. for the Gaussian profile the parameter needed is the σ_x and σ_z that correspond the the σ of the two dimension, Figure 3.2a show a code example to define a Gaussian spot of a Beam having $25 * 10^3$ rays with the two σ different, $\sigma_x = 0.1mrad$, $\sigma_z = 1mrad$ as it is showed in Figure 3.2b.

```

1  from monwes.Beam import Beam
2
3  beam = Beam()
4  beam.set_gaussian_spot(1e-4, 1e-3)

```



(a) Example code for a Gaussian source
in spatial coordinate

(b) Plot of Figure 3.2a

Figura 3.2: Example 1

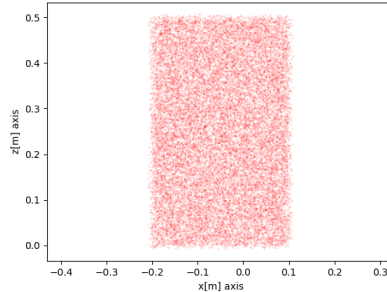
Over the Gaussian profile, there are other two geometrical profile that can be defined rectangular and circular that have a uniform distribution, of the rays, in their space domain. For the rectangular distribution the parameter to define are

the xz limit of the coordinate that define the sides of the rectangle. Figure 3.3a show an example code where it is defined a circular profile with a radius of 1cm and, after, overwritten another geometrical profile having a rectangular shape, in this case the final profile of the Beam is that figured out in Figure 3.3b, a rectangular non symmetric profile with the coordinate defined in the code in Figure 3.3a.

```

1 from monwes.Beam import Beam
2
3 beam = Beam()
4 beam.set_circular_spot(r=0.01)
5 beam.set_rectangular_spot(xmax=0.1, xmin=-0.2, zmax=0.5, zmin=0.)

```

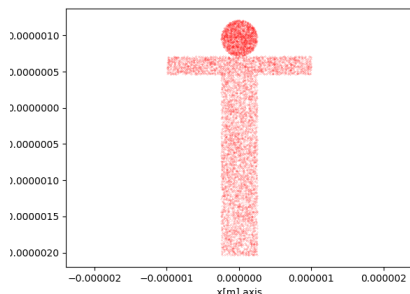


(a) Example code for a circular and a rectangular spot

(b) Example plot of the rectangular profile

Figura 3.3: Example 2

Moreover it is possible to define a special shape that have, more or less, the figure of a person with a uniform distribution of the point in all the point of the space. This special shape is showed in Figure 3.4a, that is defined in the code written in Figure 3.4b. It is used to do a test "imaging" of a system checking that the image, after the optical system, is affected by deformation or defect. As it is showed, the initialize_as_person command take two input parameter, the number of the total rays (by default are $25 * 10^3$), and a size parameter that set the coordinate limit of the figure, more precisely. In Figure 3.4a the size correspond to 10^{-6} so the limit are: $x_{max} = 1\mu m$, $x_{min} = -1\mu m$, $z_{max} = 1\mu m$, $z_{min} = -20\mu m$.



(a) Example plot "person" profile

```

1 from monwes.Beam import Beam
2
3 beam = Beam.initialize_as_person(N=10**4, size=1e-6)

```

(b) Example code for the "person" spot

Figura 3.4: Example 3

The last piece of the Beam object is the "Flag" vector. Every component of this vector have a correspondence with a certain ray and contain the information about the number of optical element that, the ray, travel until a particular moment. Moreover this value become negative when the ray doesn't hit an optical element,

in such a way to have an information where the rays were lost. Figure 3.5, resume the main parameter of the Beam object with their default values

```

8   class Beam(object):
9
10  def __init__(self,N=25000):
11
12      N = round(N)
13
14      self.x = np.zeros(N)
15      self.y = np.zeros(N)
16      self.z = np.zeros(N)
17
18      self.vx = np.ones(N) * 0.
19      self.vy = np.ones(N) * 1.
20      self.vz = np.ones(N) * 1.
21
22      self.flag = np.zeros(N)
23
24      self.N = N

```

Figura 3.5: Summary of the Beam object parameter

A part from the principal characteristic treated above, Beam object contain other option in order to manage better the utilization of it. The other option defined are reported here below:

- import_ from_ file(filename='filename'): define a Beam with a characteristic defined in a file '.h5'
- set_ point(x,y,z): move the Beam in a part of the space centred in the coordinate (x,y,z)
- initialize_ from_ arrays(x, y, z, vx, vy, vz, flag): define a Beam with the spatial value defined in the array x,y,z, the velocities' value defined in the array vx,vy,vz and the flag value defined in the array flag
- duplicate(): duplicate a Beam
- good_ beam(): define a Beam that, starting from another Beam, extract only the good rays (those that have a positive flag)
- part_ of_ beam(indices): define a Beam that, starting from another Beam, extract the ray that correspond to the position defined in the array indices
- number_ of_ good_ rays(): return the values of the good rays
- merge(beam2): merge a beam1 with another beam2, the first part of this new beam correspond to the beam1, and the second part to the beam2
- retrace(distance): this correspond to a free propagation in the space of the Beam within a distance equal to "distance"

At the end there are the command that plot the various characteristic of the beam, that contain the information for the plotted characteristic, for example plot_ xy() make a plot of the x and y coordinate of the beam, plot_ good_ xpzp() make a plot of the x-velocities and z-velocities of only the rays that have a positive flag

3.2 Optical Elements

Because, as discussed in Chapter 1, mirrors are the principal elements used in synchrotron the main optical element developed is the mirror, but it is also defined an ideal lens that is useful to simulate some particular profile for the Beam. that corresponding to this , more attention is focused on them, on the contrary , for testing uses, only one kind of lens, an ideal lens, is implemented.

3.2.1 Mirrors and lens

The different kind of mirror that are defined are:

- plane mirror
- sphere mirror
- ellipsoidal mirror
- paraboloidal mirror
- hyperboloidal mirror

All those geometrical shape are a subset of a surface conical figure. As is discussed in Chapter 2, and reported in Equation 3.1, a surface conic is defined by a series of coefficient.

$$a_0x^2 + a_1y^2 + a_2z^2 + a_3xy + a_4yz + a_5xz + a_6x + a_7y + a_8z + a_9 = 0 \quad (3.1)$$

The parameter needed to define the correct surface conic shape that define uniquely the mirror desired are:

- focal distances
- angle of incidence ϑ_g , more precisely the program use the complementary angle of ϑ_g that is $\vartheta = \frac{\pi}{2} - \vartheta_g$ (the input and output angle are in radiant)

Moreover, the surface conic, is defined in such a way to have the origin equal to the incidence point of a collimated ray distant p (that correspond to the object focal distance) from the mirror, and with the normal of the surface corresponding to the z-axis, as it is showed in Figure 3.8. For the plane mirror the situation is simple, because the equation of the surface is that in Equation 3.2, that have all the coefficient equal to 0 apart from a_8 that is equal to 1.

$$z = 0 \quad (3.2)$$

For the spherical case, the parameter that characterize a sphere is the radius, one time defined the radius, the equation of the sphere is:

$$x^2 + y^2 + z^2 = r^2 \quad (3.3)$$

Moreover, it is known, from the spherical lens optics (see Chapter 2) , that:

$$\frac{1}{p} + \frac{1}{q} = \frac{2}{r_t \sin \vartheta_g} \quad (3.4)$$

and

$$\frac{1}{p} + \frac{1}{q} = \frac{2 \sin \vartheta_g}{r_s} \quad (3.5)$$

where r_t , is the tangential radius, and r_s is the saggital radius. The sphere case have $r_t = r_s$, this mean that, apart from the normal incidence case, the sphere cannot perfectly focalize/collimate a beam. The radius chosen in Surface conic object is that corresponding to the equation 3.4:

$$r = \frac{2}{\sin \vartheta_g} \frac{pq}{p+q} \quad (3.6)$$

where p correspond to the object focus length, q to the image lengths, ϑ_g to the incidence angle.

For the paraboloid shape, to find the correct coefficients that define the right surface, it is needed the incidence angle, one focal distance and another parameter that distinguish between the two behaviour of the mirror that are showed in Figure 3.6a and, Figure 3.6b. This two system correspond mirrors that, physically, have different behaviour, the first one Figure 3.6a, focalize a Beam, the second one, Figure 3.6b, collimate a Beam.

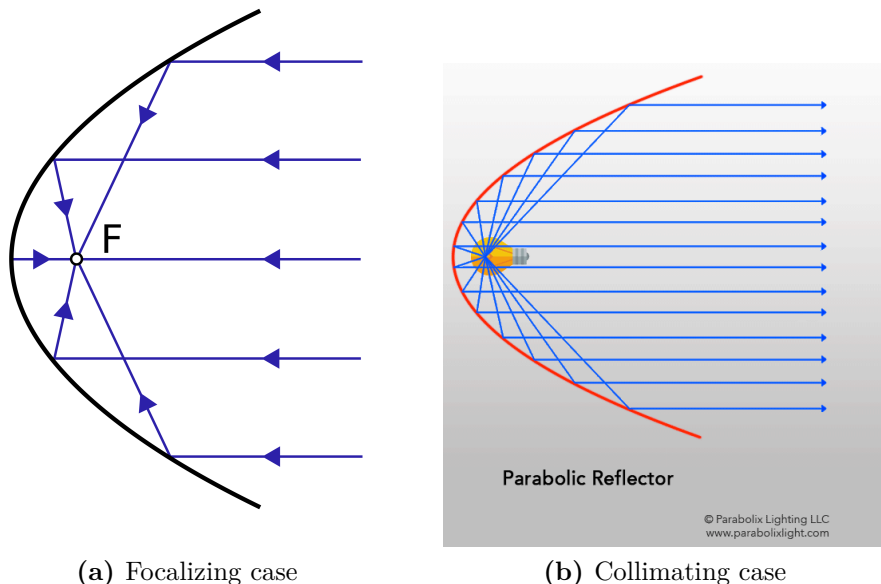


Figura 3.6: Parabola

The general equation of a parabola, such that in Figure 3.7 is

$$y = \frac{1}{4f} x^2 \quad (3.7)$$

where f is the focal distance of the parabola. After a few calculation, see Appendix B, it is possible to correlate f with the input parameter in this sense

$$f = d \sin^2 \vartheta \quad (3.8)$$

where d is the object focal distance, in the case depicted in Figure 3.6a, otherwise, in the case depicted in Figure 3.6b, d is the image focal distance.

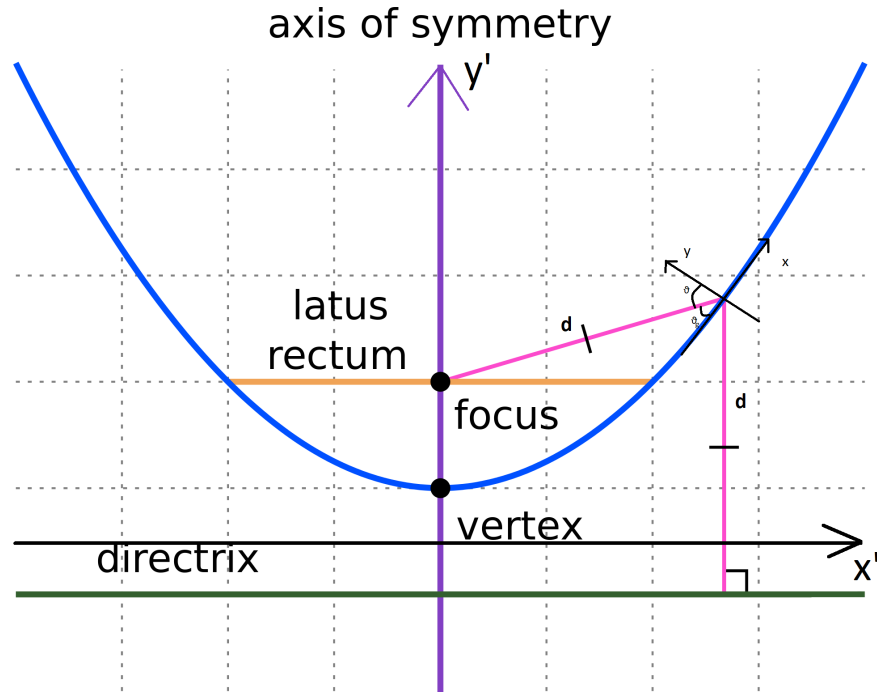


Figura 3.7: Part of a parabola (blue), with other characteristic (different color) [Wik18]

For the elliptical case the situation is represented in Figure 3.8. Equation 3.9 describe the general equation of an ellipse where appear two unknown a and b .

$$\frac{x^2}{a^2} + \frac{y^2}{b^2} = 1 \quad (3.9)$$

It is possible to correlate (Appendix B), the focal distances plus the incidence angle with the two parameters a and b with the following two equations:

$$p = \frac{a + b}{2} \quad (3.10)$$

$$q = \sqrt{ab} \cos \vartheta \quad (3.11)$$

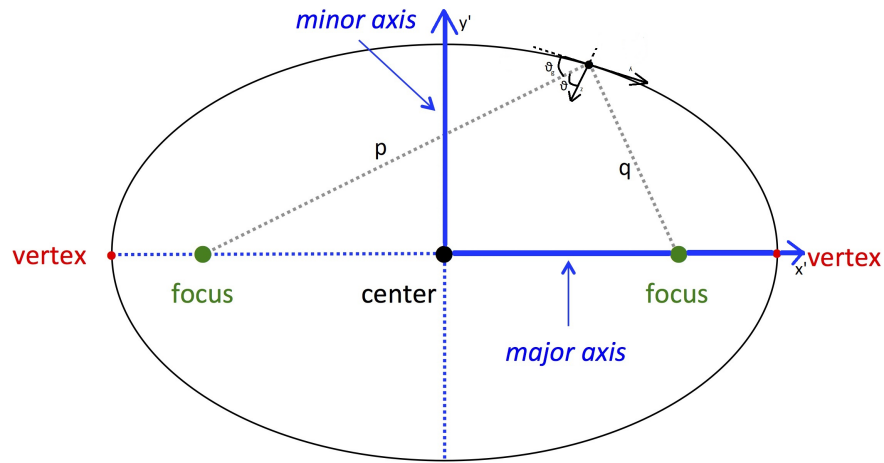


Figura 3.8: Ellipse System

Defined the surface in the $x'y'$, it is done a rotation and a translation in order to center the new xy system on the point P with the normal at that point equal to the z-axis.

For the hyperboloidal mirror the situation is similar to that of the ellipsoidal case, in fact, the general equation of the an hyperbola such the one in Figure is

$$\frac{x^2}{a^2} - \frac{y^2}{b^2} = 1 \quad (3.12)$$

and the equations that correlate the focal distances and the incidence angle with the parameter a and b are

$$p = \frac{a - b}{2} \quad (3.13)$$

$$q = \sqrt{ab} \sin \theta \quad (3.14)$$

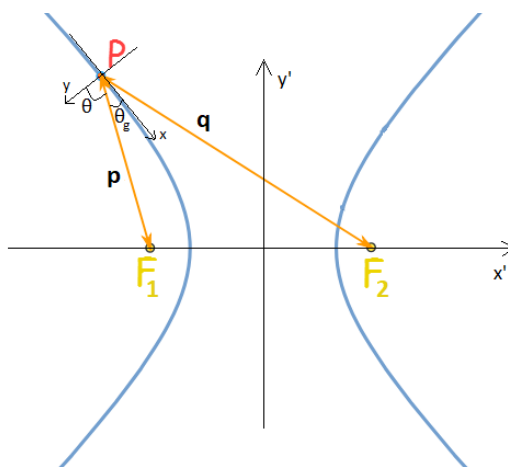


Figura 3.9: Hyperbola System

After that it, as in the case of the ellipsoidal mirror, it need a rotation and a translation to complete the work. For the mirrors, in the program, there is a further

option that make the mirror cylindrical in one dimension maintain its surface conic in the other, to do this, in Surface_conic object, it is defined a function set_cylindrical, that change the shape of the surface, from a complete surface conic, to a surface conic in one dimension and cylindrical in the other.

In addition of the mirrors elements is implemented also an ideal lens element that follow the typical lens equation:

$$\frac{1}{f_x} = \frac{1}{p} + \frac{1}{q} \quad (3.15)$$

$$\frac{1}{f_z} = \frac{1}{p} + \frac{1}{q} \quad (3.16)$$

where f_x is the x focal length and f_z is the z focal length. For this optical element the input parameters are the object focal distance, image object distance and the two focal distances (f_x, f_z) that, in the default mode, are set equal with a value equal to $f_x = f_z = \frac{pq}{p+q}$.

3.2.2 Compound Optical Element (KB and Montel system)

This program include also two different system composed by more mirrors. Starting from conical mirrors, combining them, is possible to have a compound optical elements that can simulate the behaviour of some typical instrumentation that characterize the facilities, in particular in the synchrotron world. The compound optical system implemented are two of those mentioned in Chapter 2:

- KirkPatrickBaez system (KB system)
- Montel

3.2.3 Compound System: KirkPatrickBaez

KirkPatrickBaez or, more simply, KB system are shown in Figure 3.10 is composed by two cylindrical surfacing conic mirror placed one after the other with the two focal lens that converge in the same point. There are implemented two different kind of KB system, a first one composed by two elliptical mirrors and a second one composed by parabolic mirrors. The input parameter that the program need are the two incidence angle and the two focal, with respect to the center of the KB system, represented in Figure 3.11 and the separation of the two mirror, from center to center.

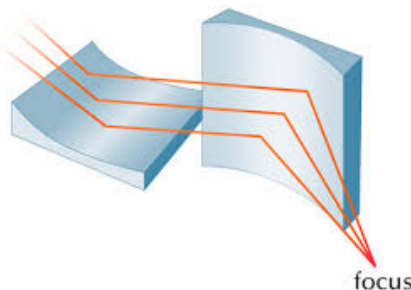


Figura 3.10: KB system

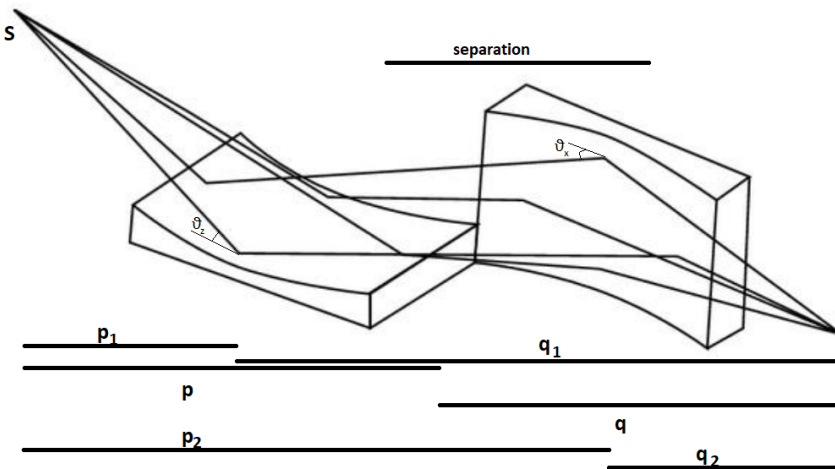


Figura 3.11: Different object/image focal length that characterize the whole KB system, and the single mirrors. Is it also showed the separation length between the two mirror

Because this system is simply a system composed by two surface conical mirror in series the parameter that the system need to define the mirror are not the ones defined by the user but are the focal distance of the two mirrors that are, as shown in Figure, p_1 , q_1 , p_2 , q_2 , These parameter represent the object focal distance (p_1 , p_2) and the image focal distances (q_1 , q_2) of the two mirror, as represented in Figure 3.11. Figure 3.12, show an example of the definition for a KB system that have an object focal length of 2m, an image focal distance of 5m, a separation between the two center of the mirrors of 1m, and the two angle of incidence equal each other to 2° .

```

1  from monwes.CompoundOpticalElement import CompoundOpticalElement
2  import numpy as np
3
4  theta = 88. * np.pi / 180
5  KB = CompoundOpticalElement.initialize_as_kirkpatrick_baez(p=2., q=5., separation=1., theta_z=theta)

```

Figura 3.12: Example 5

3.2.4 Compound System: Montel

The Montel system, depicted in Figure 3.13, is composed, as for the KB, by two surface conical mirror cylindrical in one direction, but, because the two mirror are not in series, as for the case of the KB, the situation is a bit complicate. Starting from definition of the two mirrors one is rotated of 90° , in order to have a mirror in the xy plane, and another one in the zy plane. As shown in Figure 3.13 the center of the Cartesian system is setted in the point where the optical axis of the system hit the compound system having the normal of the first normal equal to the z -axis, and the second normal equal to the $-x$ -axis. The system is defined by the following parameter p , q , ϑ_z , ϑ_x , where p and q are the focal distance of the two mirrors and ϑ_z and ϑ_x are the angle of incidence to define the correct mirrors (by default $\vartheta_z = \vartheta_x$).

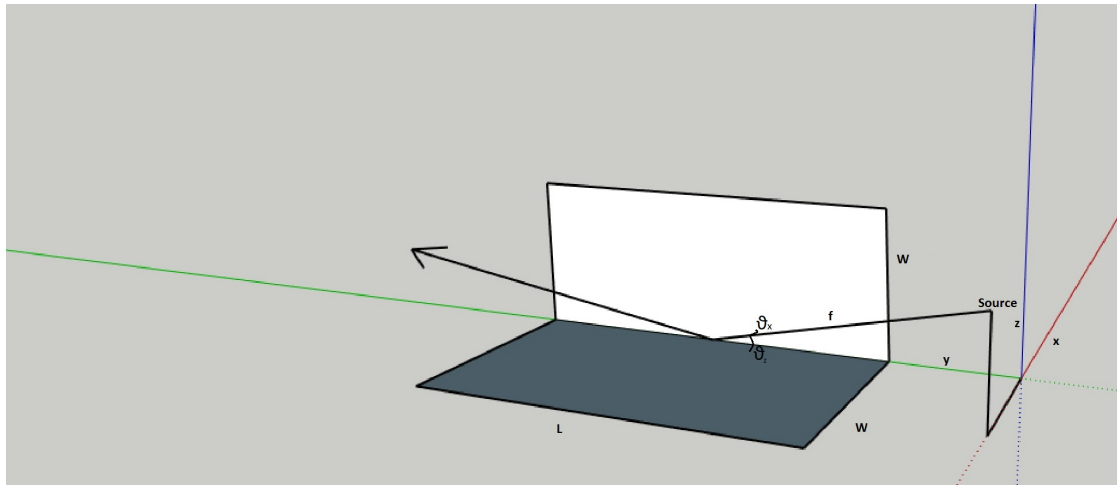


Figura 3.13: System

The following Figure 3.14 show an example code for a parabolic Montel system having an object focal length of 5m, image focal length of 2m and the two incidence angle of 1.5° , that focalize a Beam. As for the KB system also in this case there are implemented two possibilities, an ellipsoidal system (having the two mirror as ellipsoid), and parabolic system (having the two mirror as ellipsoid).

```

1  from monwes.CompoundOpticalElement import CompoundOpticalElement
2  import numpy as np
3
4  theta = 88.5 * np.pi / 180
5  montel = CompoundOpticalElement.initialize_as_montel_parabolic(p=5., q=2., theta_z=theta, infinity_location='p')

```

Figura 3.14: Example 6

3.3 Tracing System

Defined the Beam and the different optical element, to complete a simulation, is needed a tool that put everything together and modify the property of the beam after the interaction with the optical elements.

For example, if it want to simulate the system depicted in Figure 3.15, it have to define a Beam source, the optical element and, at the end, somewhere, the distances between the optical elements. The tracing part of the program, for the non-compound optical element, is written in such a way that the trace work in series, one optical element after the other. This, in series methods, work with the definition of two distances, object/image distance from the center of the optical element, the incidence angle of the Beam, that can be different from the designing one, and a second angle that define the mirror with respect to the Beam. (normally and also for the default case the incidence angle i equal to the designed one, and the second angle is fixed to 0°). One possibilities, to define the system in Figure 3.15 is to set the object distances of the mirrors equal to distance d_0 and d_1 , and the image distances equal to 0, for the lens lets set the object distance equal to d_3 and the image distance equal to d_4 as it is reported in Figure 3.16.

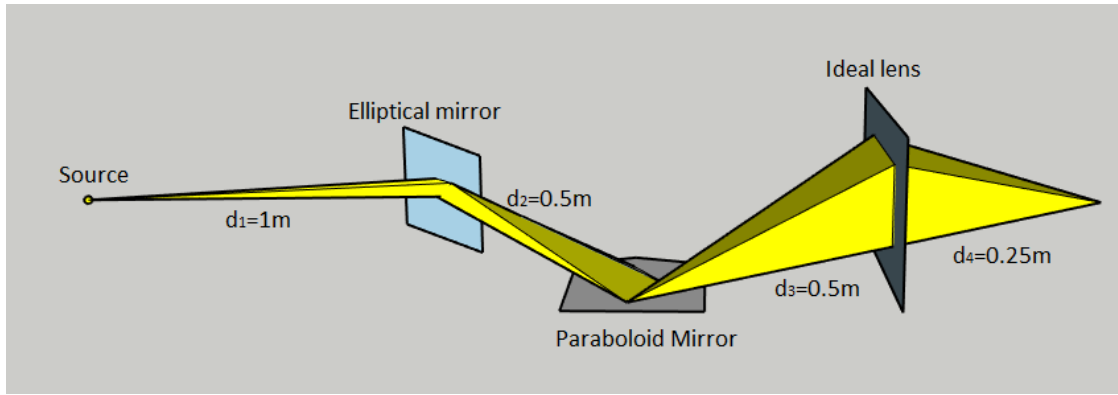


Figura 3.15: System

```

1 import ...
5
6
7 theta_e = 88.5 * np.pi / 180
8 theta_p = 88. * np.pi / 180
9 beam = Beam()
10 beam.set_gaussian_divergence(1e-3, 1e-4)
11
12 ell = Optical_element.initialize_as_surface_conic_ellipsoid_from_focal_distances(p=1., q=2., theta=theta_e)
13 par = Optical_element.initialize_as_surface_conic_paraboloid_from_focal_distances(p=0.5, q=2., theta=theta_p, infinity_location='p')
14 lens = Optical_element.initialize_as_ideal_lens(p=1., q=2.)
15
16 beam = ell.trace_optical_element(beam, p=1., q=0)
17 beam = par.trace_optical_element(beam, p=0.5, q=0., alpha=np.pi/180)
18 beam = lens.trace_optical_element(beam, p=0.5, q=0.25)

```

Figura 3.16: Example 7

3.3.1 Tracing for simple Optical element

Going deeper in the code, the algorithm that trace a single element is divided in 5 step

1. change the reference system from that of the optical axes to that of the optical element after two rotation, one along x-axis, and second along y-axis, and a translation equal to the object distance of the optical element
2. free propagation up to the optical element
3. effect of the optical element
4. free propagation to the image plane
5. changing the Cartesian system in that one that have the optical axis equal to the y-axis

The first three point are condensed in the method `effect_of_the_optical_element`, that is showed in Figure 3.17a, and the last two point are condensed in the method `effect_of_the_screen` that is showed in Figure 3.17b.

```

227     def effect_of_optical_element(self,beam):
228         self.rotation_to_the_optical_element(beam)
229         self.translation_to_the_optical_element(beam)
230         [beam, t]=self.intersection_with_optical_element(beam)
231         self.output_direction_from_optical_element(beam)
232
235     def effect_of_the_screen(self,beam):
236         self.rotation_to_the_screen(beam)
237         self.translation_to_the_screen(beam)
238         if np.abs(self.q) > 1e-13:
239             self.intersection_with_the_screen(beam)
240

```

(a) Example code for a Gaussian spot

(b) Plot of Figure 3.2a

Figura 3.17: Example 1

Because of the different definition, the tracing method of the rays' beam, need a different interpreter that can link the beam with the different optical elements that meet on his way. Because of the different nature, there are implemented two kind of tracing, a first one that trace the KB system, that is composed by a series of optical elements and so can be used for all the compound optical elements that are in series. And a second one that is specific for the Montel system, because it is not composed by mirrors in series rather than mirrors in parallel, having the two elements in a very small region of the space that have in which order the rays of the beam hit the different mirrors.

3.3.2 Tracing for KB

For KB system the situation is more or less the same as for a simple optical mirrors, with the only difference that there are more than one mirror. So the algorithm to simulate the tracing system is nothing else than a for loop, that use the tracing system of the simple optical element. In this the object and the image distance from the center of the system are the default ones, such as for the incidence angles. Figure 3.18, show the trace code for the compound elements that are in series.

```

372     def trace_compound(self,beam1):
373
374         beam=beam1.duplicate()
375
376         self.system_initialization(beam)
377
378         for i in range_(self.oe_number()):
379
380             if self.oe[i] is not None:
381
382                 self.oe[i].effect_of_optical_element(beam)
383                 self.compound_specification_after_oe(i=i)
384                 self.oe[i].effect_of_the_screen(beam)
385                 self.compound_specification_after_screen(beam = beam, i=i)
386
387         return beam

```

Figura 3.18: Example 8

3.3.3 Tracing for Montel

As said at the beginning of the Chapter, the tracing method used for Montel is new and different from the other. For the KB case the tracing method utilized is

sequential. This mean that all the rays hit firstly a mirror, and secondly the other mirror. Figure 3.19 and Figure ??, show the KB (Figure 3.19a) and Montel (Figure 3.19b and ??) situations.

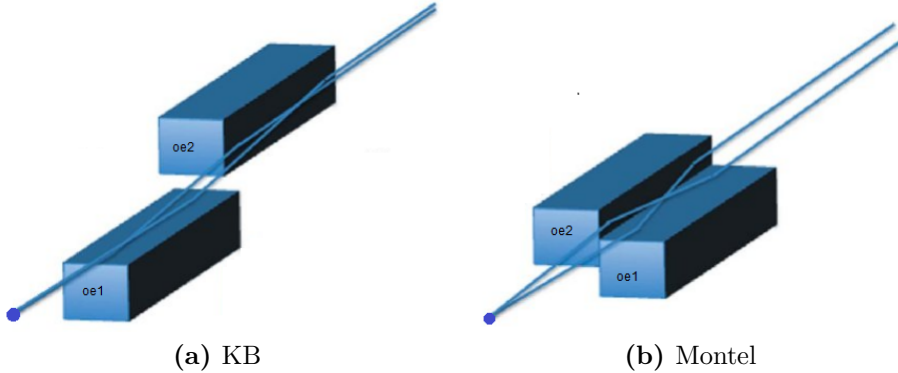


Figura 3.19: From [LIA⁺11]. For the KB system (Figure 3.19a) all the rays hit sequentially one mirror after the other. For the Montel system (Figure 3.19b) a portion of rays coming from the source hit firstly oe1 and secondly oe2, the other portion do the opposite thing.

The first step to trace the Montel is that to change the reference frame from the source optical axial to the optical system. This system is chosen to have origin in the center of whole system with the normal of the two mirror along z and -x axis, as it is showed in Figure 3.13. Moreover, the change of reference frame, has to be done in order to force the beam to have incidence angles, and distance from the center of the system equal to those chosen by the user. To do this, two rotation, that rules the values of the angles and one translation, that rule the distance between source and center of Montel. These angles and distance can be equal to the initialized values.

The second step consist in the propagation step. Because the beam hit simultaneously the two mirror a new method is implemented. This method, named comparison_time, compare the time that each ray take to reach the different mirrors. Calculated the time for each ray, is set a flag that specify the closest optical element. At this point the Beam is divided in three "sub-Beams", a first one that contain the rays going to the first mirror, a second one that contain the rays going to the second mirror, and a third one that contain the rays that, because of the finite size of the mirrors, doesn't hit any mirror. At this point each sub-Beam is traced to the corresponding optical element and so are computed the effect of the mirror on the 1st and 2nd sub-Beams. This process gives three output: "beam1", "beam2" and "beam3". These output contain the information of the beam along the whole propagation system.

The "beam1" and "beam2", are list of two dimension that contain the rays of that will hit the first mirror at the first and at the second iteration. "beam3" is the most important output, because contain the information of the beam at the image plane. This list is divided in three Beam, where the first beam contain the information of the ray that undergo no-reflection, the second Beam contain the information of the ray that undergo one-reflection and the third contain the information of the

ray that undergo two-reflection. Figure 3.20, show the spatial coordinate of the three element of the "beam3", where the red dots correspond to the beam with no-reflection, the blue dots correspond to the beam with no-reflection and the green dots correspond to the beam with no-reflection.

The last step of this tracing method consist in a re-change of reference frame to the optical axis of the two reflected beam (as showed in Figure 3.20, where the green dots are centred in the point (0,0)). This transformation is similar to the first step of this tracing method where the two reflection are done with respect to the same angle of incidence, and the translation depend on the value set by the user corresponding to the distance from the center of the Montel system.

Here below a brief summary of the tracing method:

1. Changing the reference frame from the source optical axis to the Montel system
2. Focus the attention on the travel time of each ray in order to know which is the nearest optical element of each ray
3. free propagation of each ray up to the nearest optical element
4. effect of the system for each ray
5. repeat the 2nd, 3rd and 4th passage two times, in order to consider the two reflection
6. Change the reference system to the optical axes that is subject to two reflection, doing two rotation and one translation

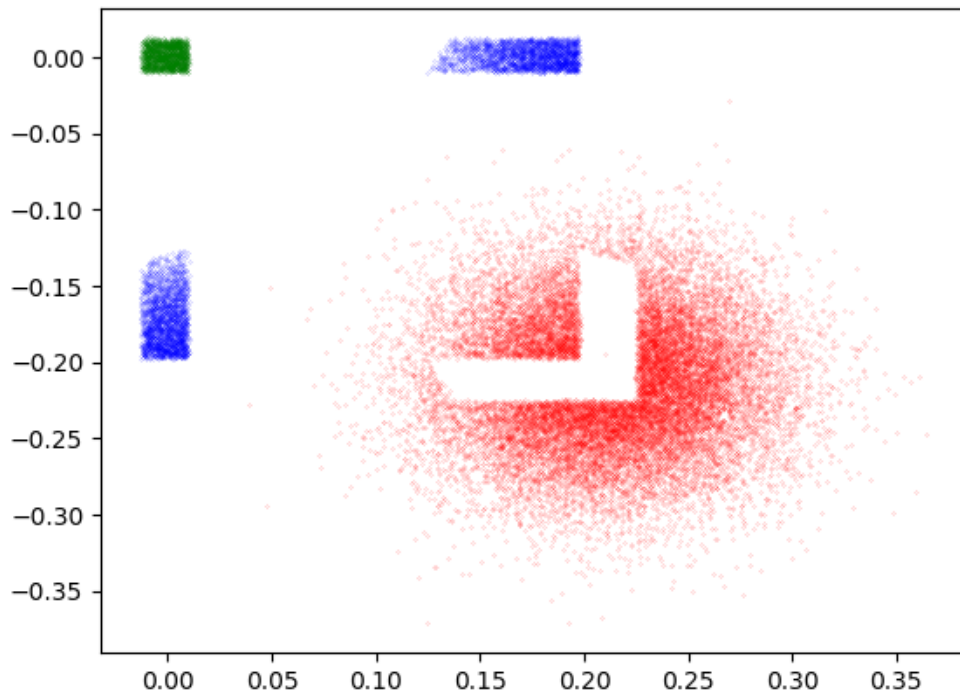


Figura 3.20: Example 8

Because of the importance of the Montel system in my Thesis, it is implemented some additive option with the aim to study better the behaviour of the system.

These new parameters that affect the tracing system are:

1. focal distances and incidence angles, that define the two rotation and the translation of the tracing system
2. name of the File in which is saved the data of the simulation, by default no data is saved
3. there is the possibility to choose a different point, from the origin, in which the optical axis hit the system
4. there is also the possibility to have a final output frame that is not solidal by the two-reflected beam, but with the non reflected beam or with the other two beam that are reflected only one time
5. It is also the possibility to figure out the footprint of the two reflected beam on the system. For clarity the beam that hit the first mirror and after the second is labelled with red point, the beam that hit the second and after first mirror is labelled by blue color

In Chapter 4, these option will be useful in the comprehension of the Montel. The possibilities to change the angle of incidence and to hit different part from the origin can be used to study what happen to a beam when is not aligned, or not perfectly aligned, and use these result to align the system in the laboratories. The possibilities to save a File is useful in particular in those case where there is a huge computational effort that need a lot of time, in these cases is possible to work with the result of a big simulation without reappointing it, and so save time. Figure 3.21 show the code that trace a Montel elements, containing also the special option that were defined above.

```

681
682     def trace_montel(self, beam, name_file=None, mode=0, p=None, q=None, theta_z=None, theta_x=None, hitting_point=Vector(0., 0., 0.),
683                         output_frame=0, print_footprint=1):
684
685         self.oe[0].set_parameters(p=p, q=q, theta=theta_z)
686         self.oe[1].set_parameters(p=p, q=q, theta=theta_x)
687
688         v_in = self.get_optical_axis_in(mode)
689
690         self.input_frame(beam, v_in, mode, hitting_point)
691
692
693         beam1, beam2, beam3 = self.apply_specular_reflections(beam, name_file, print_footprint)
694
695         if output_frame == 0:
696             v_out = self.get_optical_axis_out(mode)
697         elif output_frame == 1:
698             v_out = v_in
699
700         self.output_frame(beam1[0], v_out, mode)
701         self.output_frame(beam1[1], v_out, mode)
702         self.output_frame(beam3[2], v_out, mode)
703
704
705         return beam1, beam2, beam3

```

Figura 3.21: Example 8

Capitolo 4

Test and Results

In the first part of the Chapter is tested the correct working of the MONWES library. The test for mirrors, ideal lens and KB is done against OASYS software. For the Montel system, because is not implemented in OASYS, it is done a benchmark with the paper [RKM15].

The second part of the Chapter use the MONWES library to study the behaviour of the Montel system. It is studied the effect of a non-centred beam focusing on how the image dimension and the intensity change with respect to the position of the hitting point of the Beam on the system. At the end is reported the study that I have done, for the beamline ID20 of the ESRF, for a non-orthogonal Montel mirrors.

4.1 Testing against OASYS

OASYS (OrAnge SYnchrotron Suite) is a graphical environment for optic simulation used in synchrotron facilities based on orange 3, developped by Manuel Sanchez Del Rio (ESRF) and Luca Rebuffi (ELETTRA). The comparison between the program and the OASYS software is done with the system in Figure 4.1, where the 1st optical system collimate the source, the 2nd optical system focalize the mean at the image plane, the system between the source and the 1st optical system correspond to the focal distance of the system $d_1 = f = 0.4m$, between the 12st and the 2nd optical system with a distance $d_2 = 0.6m$ and the distance between the 2nd system and the image plane correspond to the focal length of the 2nd optical system that is $d_3 = f = 0.4$. A system that have parameters defined as before,

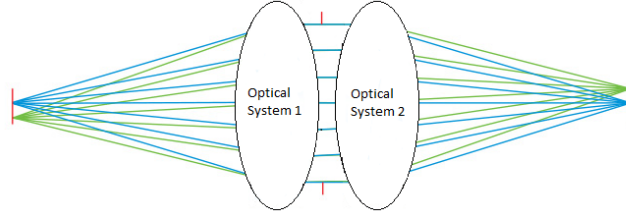


Figura 4.1: Optical system used for the test with OASYS

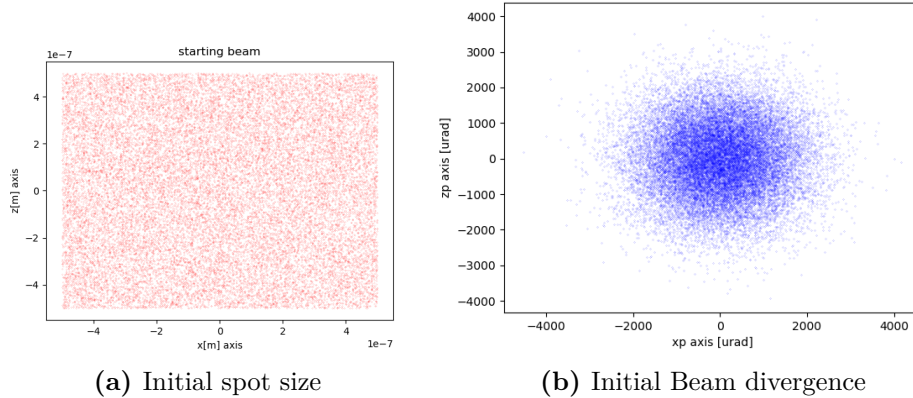


Figura 4.2: Parameter of the source used for the test with OASYS

make a copy of the source image at the image plane. The source parameter used are showed in Figure 4.2, and correspond to a square source spot of $1\mu\text{m}^2$, and a initial Gaussian divergence with a FWHM of 1mrad . The tests are done using different optical system, with the same focal length and, for the mirror it is used a grazing incidence angle of $\vartheta = 1.719^\circ$. Below are plotted the image of the Beam at the image plane, putting the OASYS' results on the right, and my results on the left. The system simulated are done with:

1. ideal lenses Figure 4.3
2. parabolic mirror Figure 4.4
3. KB system Figure 4.5

As it is showed in the figures, the result are pretty similar, with an image that depend on the kind of the system. The ideal lenses case show a perfect image, on the contrary, KB and paraboloid, show similar images but a bit ruined degrades by the propagation.

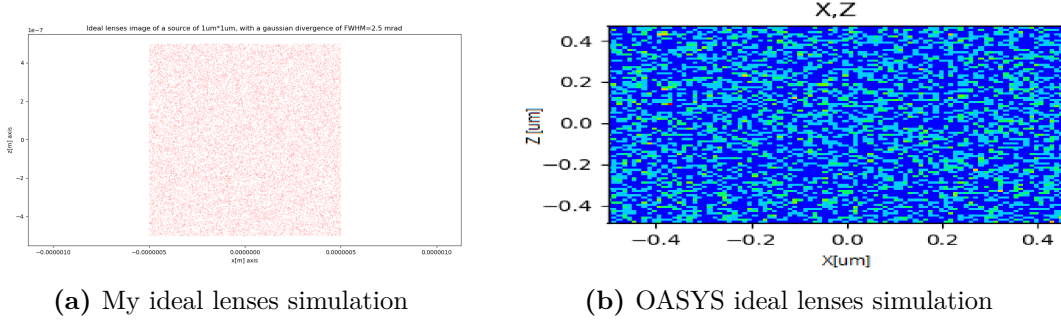


Figura 4.3: Image for the testing ideal lenses system in Figure 4.1 of: my simulation (Figure 4.3a) and OASYS simulation (Figure 4.3b)

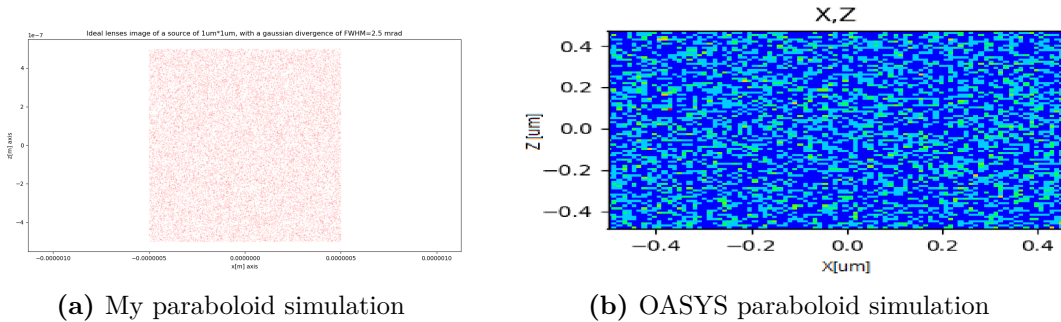


Figura 4.4: Image for the testing paraboloid system in Figure 4.1 of: my simulation (Figure 4.4a) and OASYS simulation (Figure 4.4b)

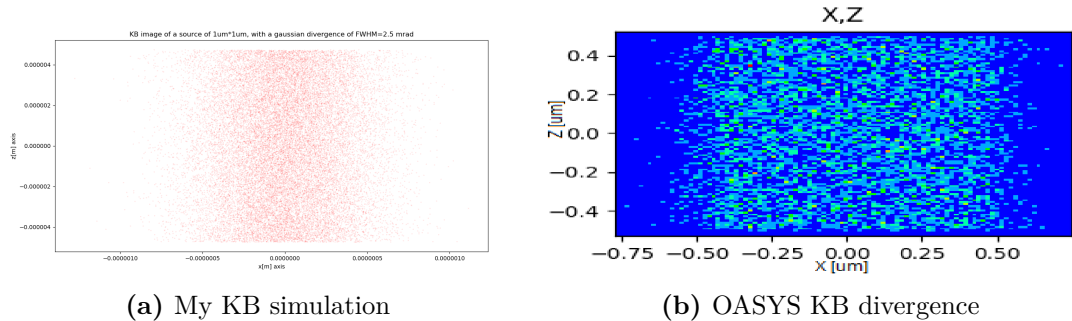


Figura 4.5: Image for the testing KB system in Figure 4.1 of: my simulation (Figure 4.5a) and OASYS simulation (Figure 4.5b)

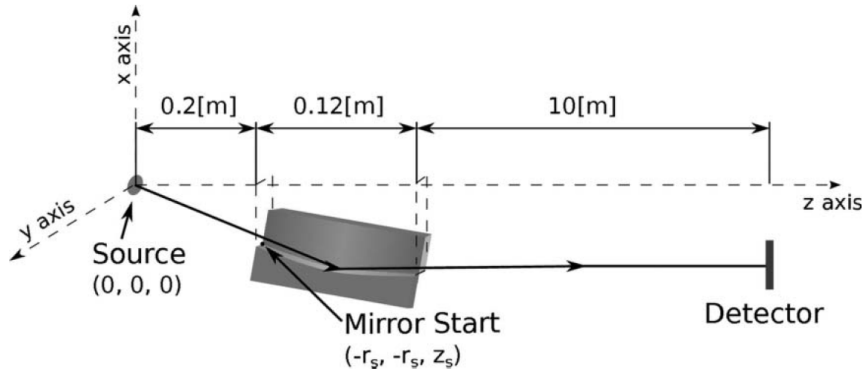


Figura 4.6: Illustration of the Montel system used as a collimator in the paper [RKM15]

4.1.1 Benchmarking

In Figure 4.6 is depicted the Montel system used in the simulation done by the paper in its system of reference. The aim of this system is to collimate a Beam using a Montel with two parabolic mirrors. The source used have a Gaussian dimension with a FWHM of $2.5\mu\text{m}$ and a Gaussian divergence of 5mrad . The distances, between the source/image plane and the center of the Montel are, respectively, $\simeq 0.26\text{m}$ and 10.06m , moreover, the incidence angle of the Beam is $\vartheta_g \simeq 2.86^\circ$. The result, at the image plane, of the beam size and beam divergence, after the double-reflection of the Montel system, is showed in Figure 4.7. Where, in Figure 4.7a, is showed the figure of the beam at the image plane, and, in Figure 4.7c, is showed the divergence. The quantitative values reported on the paper correspond to a Gaussian-like distribution with a spacial FWHM of $\sim 0.7\text{mm}$, for the spot size, and a FWHM of the Gaussian divergence $\sim 0.01\text{ mrad}$.

Repeating the simulation with my program using the parameter defined in in the paper [RKM15], are figured out in Figure 4.7. As it is showed in the Figure 4.7 there are a qualitative good agreement with the two simulation .Also, under a quantitative point of view, there is a good agreement in fact, in my simulation are obtained a value of $\sim 1\text{mm}$ of FWHM of image size, pretty similar to the one of the other simulation, and $\sim 0.01\text{ mrad}$ FWHM of divergence that is equal to the one obtained with the other simulation.

4.2 Analysis of Montel system

In this section it is done, using the Montel tools developed, a study of the Montel effect with respect to a Beam, simulating different situation. The first point, to understand if Montel work well, is to simulated the behaviour of a point-wise source with a certain divergence, using a collimating system, and watching what happen to the beam. The second step is to simulate a collimating beam with a certain source shape geometry and figure out the image plot obtained by a focalizing system in its image plane. What is expected is a point, in the velocity space for the first situation and in the real space for the second simulation, as a consequence of the ideal collimating/focalizing system. For the simulation are used parabolic Montel

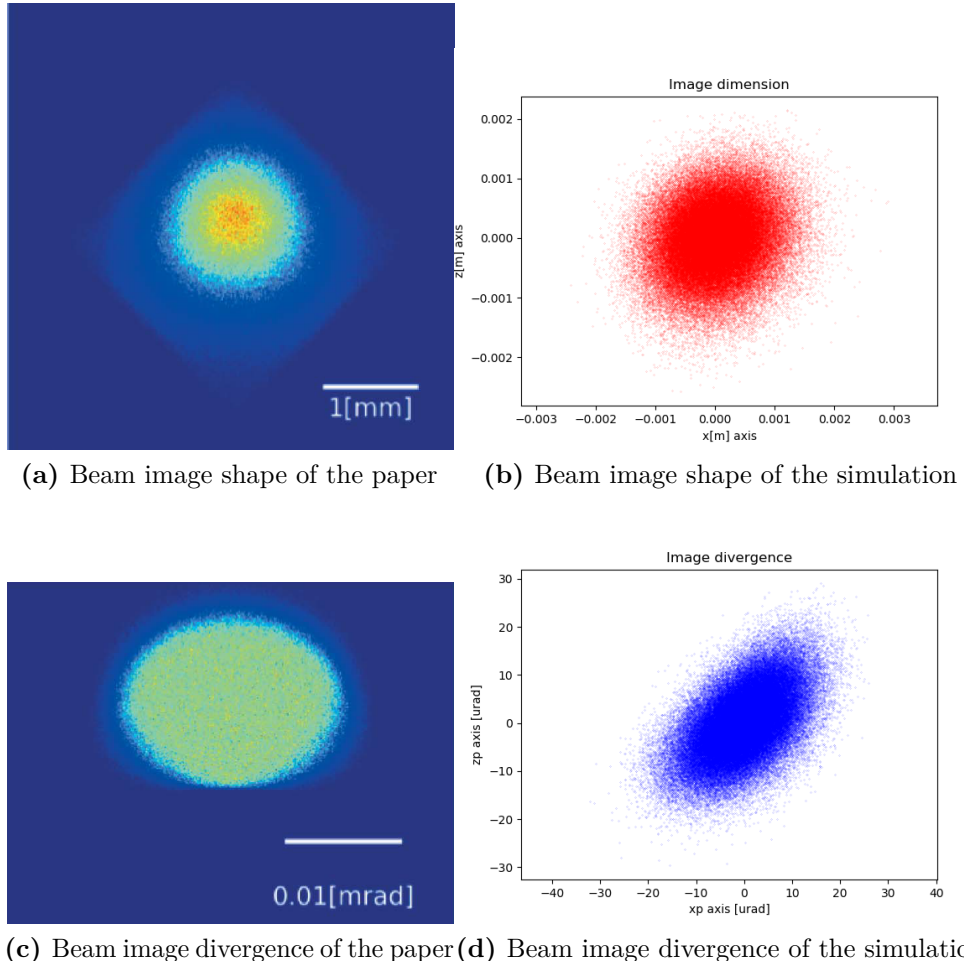


Figura 4.7: Results of the Montel simulations with a source beam with a FWHM spot of $2.5\mu\text{m}$ and a Gaussian divergence of 5mrad

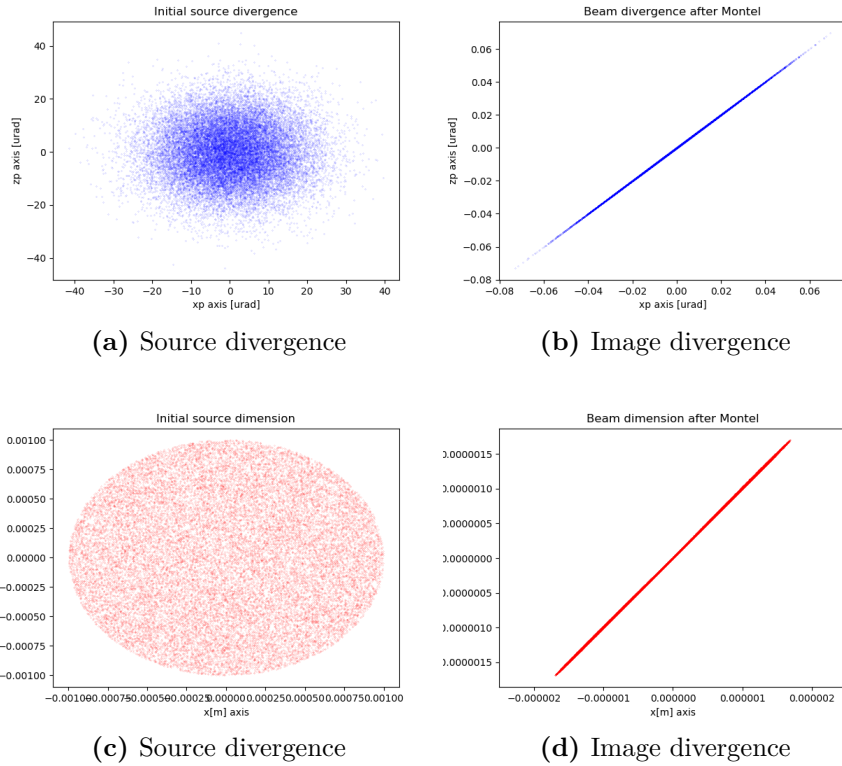


Figura 4.8: Ideal system

with an incidence angle of 2° (the choice of the angle is arbitrary. Parabolic system are chosen because is the only way to obtain a perfect collimating Beam).

In Figure 4.8 are reported the result for the ideal collimating/focalizing cases. For the collimation system is used a point wise source with a Gaussian divergence of FWHM of $25\mu\text{m}$, 4.8a. At the image plane the Beam (Figure 4.8b) is collimated, reducing its divergence of 3 order of magnitude. For the focalizing system, it is used a circular source spot having a radius of 1mm, 4.8c, with a collimated source beam. At the image plane the dimension of the Beam (Figure 4.8d) is reduced of 3 order magnitude. It is possible to conclude that both collimating and focalizing system work but not perfectly (the final results are not point). One explanation can be that, because of the particular configuration of the mirrors of the Montel, the effect on the Beam are not perfect. This can be an **intrinsic aberration of the Montel**, that can be studied more in the future.

Up to now the dimension of the Montel were not considered. The Montel is set to have infinite dimension in all the direction. This approach hold in the case of a small source and a narrow profile divergence, that hit only a small part of the system. Otherwise, for example of an isotropic source that can be modelled with a very big divergence, the situation change. In this part, to study the behaviour of a big source, it is used a Beam source with a square shape with a side of 1mm, with a Gaussian profile divergence of FWHM=1mrad. These parameter show what happen to the Montel where it is covered over all its surface. In this case a focalizing parabolic Montel is used with: object distance of 1m, image distance of 3m, incidence angle

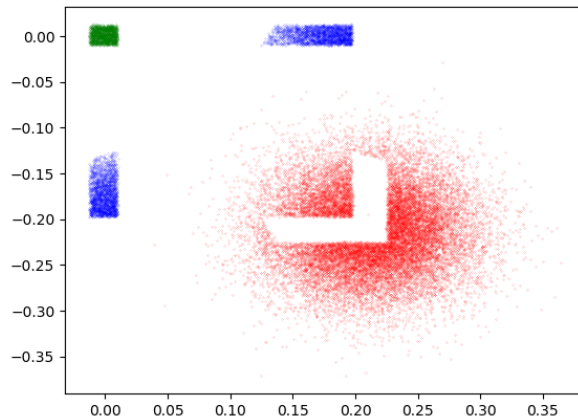


Figura 4.9: Illumination at the image plane of the different Beam (red dots correspond to np-reflected rays, blue dot to one-reflected rays, green dots to two-reflected rays).

of 2° , length of the Monte of 0.1m and width of the Montel of 20cm. Figure 4.9, show thee image plane of the Montel defined above. This plot show 4 figure, the biggest one, represented by the red dots, correspond to the rays that reach the image plane without touch the Montel, the rays coloured in blue, are those which are subject to only one reflection that are positioned in different part of the image plane depending which mirror meet, those that hit the xy-mirror correspond to the beam elongated along z, the zy-mirror correspond to the beam elongate along x. At the end, the green dots, are the rays that do both reflection and are centred to the center of the image plane by definition of it.

4.3 Non-centred Beam

In this section is studied the effect of a Montel system of a non centred-Beam in order to understand how to align correctly beam. The alignment study is study simulating a beam tha hit different point of the Montel. Is reported the behaviour about the change of FWHM of both x' and z' , of a small ($1\mu m^2$) source with a narrow divergence ($25\mu rad$), following different path. Figure 4.10 show the different path followed to simulate the non-centred. Every path is labelled with a name:

1. Y
2. XZ
3. XYZ1
4. XZY2

The system used is a focalizing parabolic Montel with an object focal distance of 0.2m and an image focal distance of 0.9, working on miroor designe for incidence angle of $\alpha_g = 2^\circ$. Figure 4.11 show the result the two FWHM of the beam changing

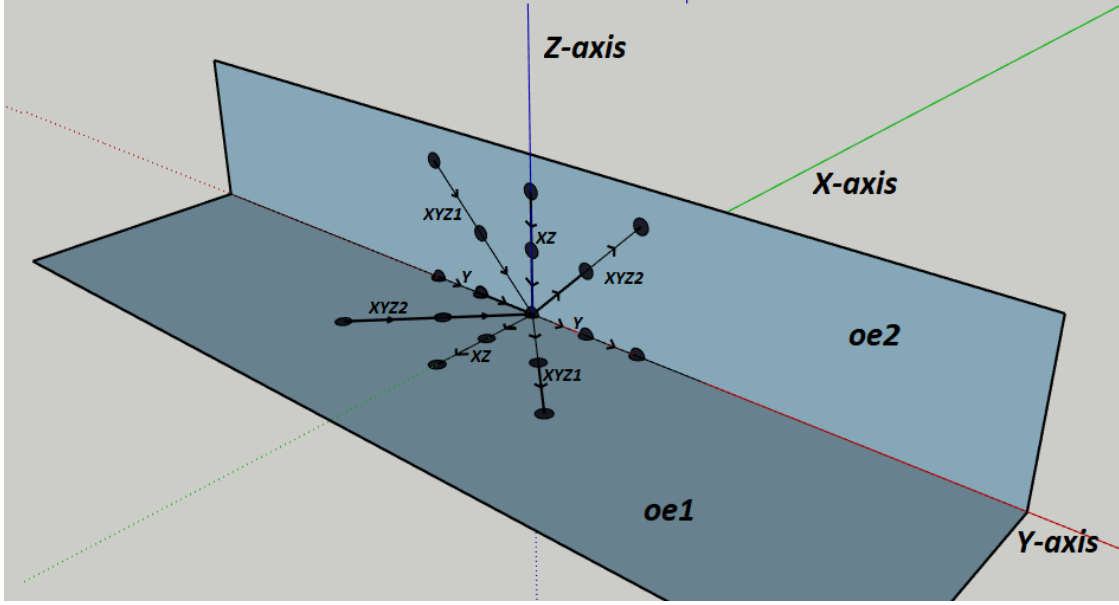


Figura 4.10: Different path for simulate the non-centred beam

the incidence point of the beam moving the different paths. This point is defined with respect to the center of the Montel system that correspond to the origin (0, 0, 0). In Figure 4.12a, the incidence point move along y-axis, start from the point (0, 1.5mm, 0) and arriving to the point (0, -1.5mm, 0), and show, more or less, a flat behaviour of the FWHM. Figure 4.12b start from the point (0, 0, 0.15mm) and arrive to (-0.15mm, 0, 0) and have specular behaviour for the two FWHM, there is a minimum of the two FWHM near the origin point, moving on the oe1 worse the FWHM of z' and maintain the other constant, on the contrary, moving on the oe2 the situation is reversed, in this case the FWHM of x' get worse, maintaining constant the one of z' . Figure 4.12c start from (0, 1.5mm, 0.15mm) and arrive to (-0.15mm, -1.5mm, 0) and Figure 4.12d start from (-0.15mm, 1.5mm, 0) and arrive to (0., -1.5mm, 0.15mm). The behaviour of this last two path are similar to that of 4.12b, this is reasonable, because the motion along y-axis does not influence the FWHM because of the definition of the cylindrical mirror, that in any point along the y direction have the same geometry.

In Figure 4.12 it is show the intensity profile of the two-reflection beam of source with a 10mm^2 of area and a Gaussian divergence of $\text{FWHM} = 25\mu\text{rad}$. In this case the Montel used is the same as before but with a length of 20cm and a width of 2cm. The intensity is calculated as the number of the rays in the two-reflection beam with respect to the initial number of rays. The different path move along these points; $y_{\max}=50\text{cm}$, $y_{\min}=-50\text{cm}$, $x_{\min}=-2\text{cm}$, $x_{\max}=0$, $z_{\max}=2\text{cm}$, $z_{\min}=0$. The plots in Figure 4.12, are interesting, because represents the intensity of the "green" Beam in Figure 4.9, that can be directly measured and so, it is possible to relate the centring of the Beam calculating the intensity of this Beam.

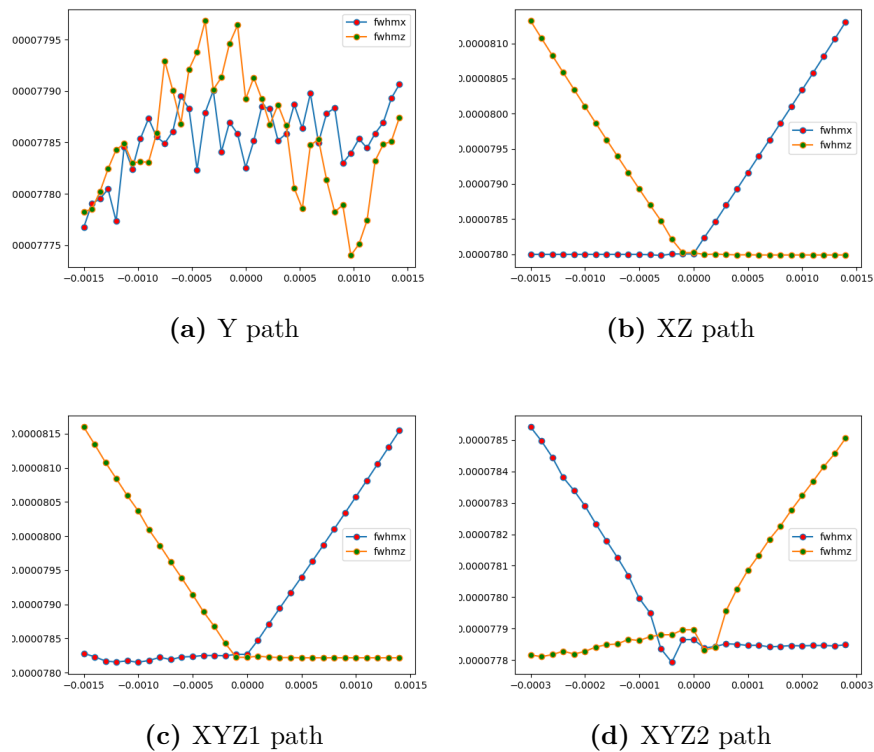


Figura 4.11: Results of the Montel system of a source beam with a FWHM spot of $2.5\mu\text{m}$ and a Gaussian divergence of 5mrad

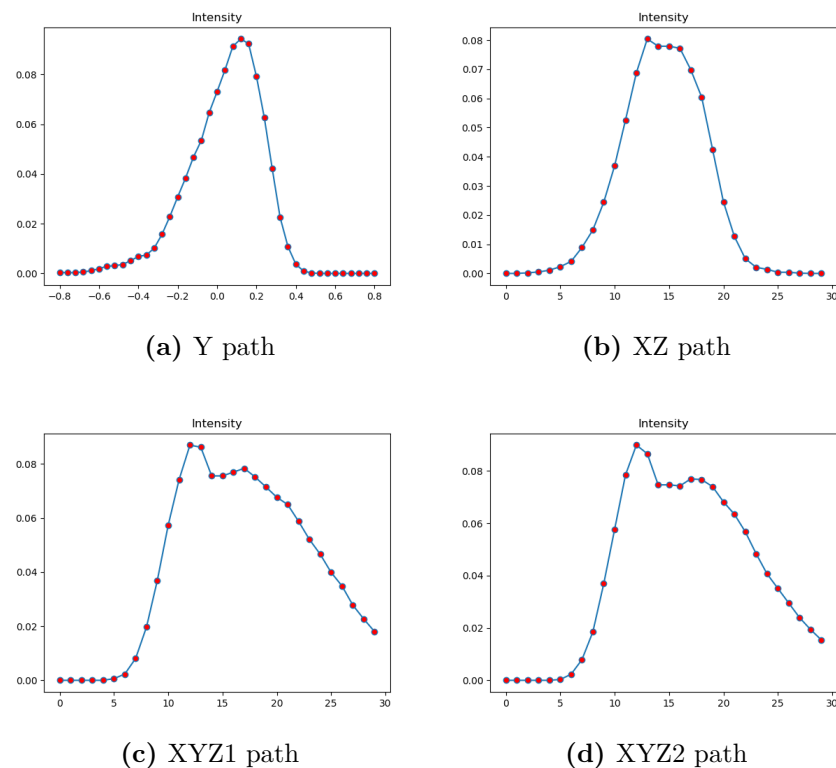


Figura 4.12: Results of the Montel system of a source beam with a FWHM spot of $2.5\mu\text{m}$ and a Gaussian divergence of 5mrad

4.4 My work for the ID 20

In this section is reported the study that I have done for the beam of ID20 of the Esrf. The simulation were done in order to study the

4.4.1 System parameters

The system simulated have a source size of $1\mu m^2$ (see Figure 4.13a) with a Gaussian divergence of $25\mu rad$ (see Figure 4.13b). The parameters of the system are: object distance of $351mm$, mirror Length of $300mm$, mirror width of $100mm$, the error max between the orthogonal configuration of the two mirror is of $\Delta = \pm 0.03^\circ$ and an incidence angle of $18.1mrad$. In Figure 4.14 is showed a 3D graphic view of the Monter system with the parameter used.

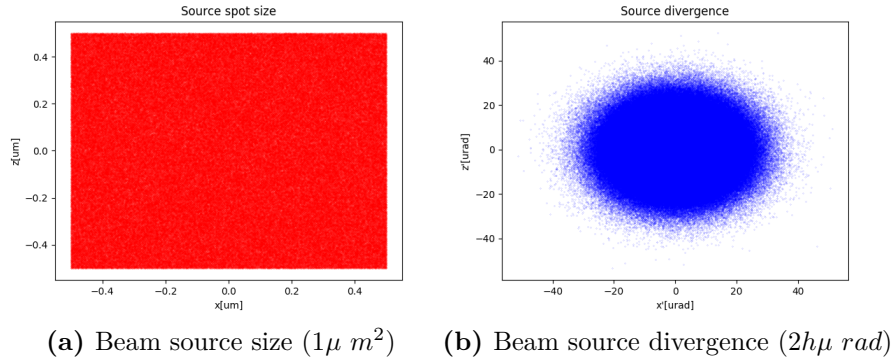


Figura 4.13: Source parameters used for the study of the Montel Analyser for ID20

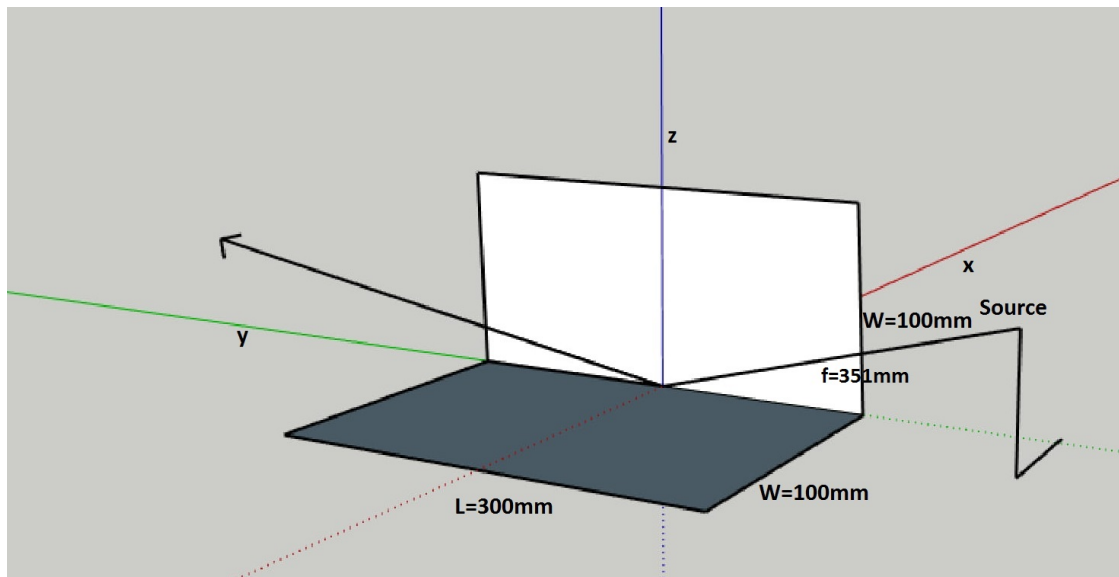
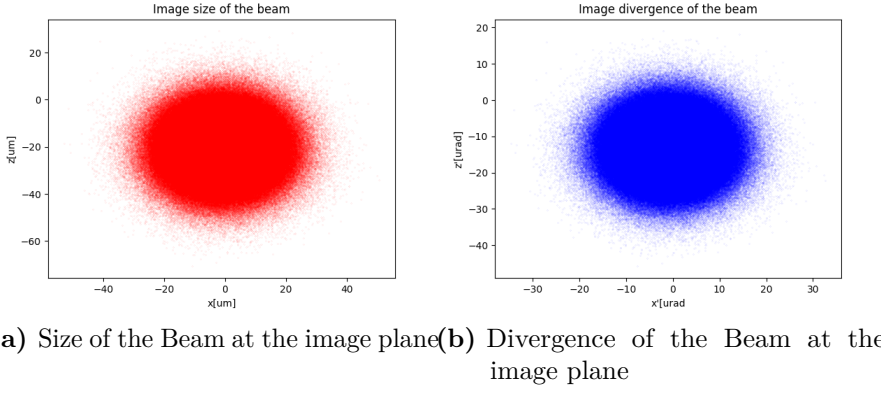


Figura 4.14: Montel parameters used for the simulation for ID20

4.4.2 Result of beam figure and footprint

The image plane is positioned at $1m$ from the center of the Montel system. The property of the beam at the image plane are showed in Figure ?? . It is obtained, a new spot size with a length of $60\mu m$ in the x direction and $100\mu m$ in the z direction, and the divergence has a dimension of $\simeq 40\mu rad$.



Moreover is interesting to note the footprint of the two mirror (Figure 4.15) because the area hit by the beam have a greater component on the y direction (due to the grazing incidence), than in the other direction. The x-length of the xy-mirror, and the z-length of the zy-mirror, is very small (at the order of $20\mu m$) with respect to the y-length that is $\simeq 20mm$.

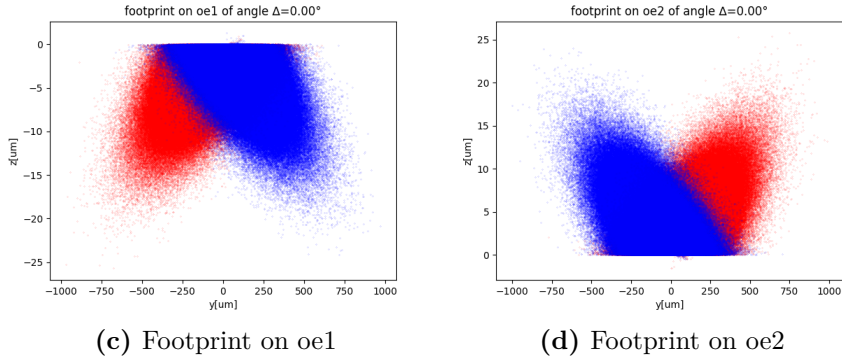


Figura 4.15: Footprint, on the xy-mirror (4.15c) and on zy-mirror (4.15d). The red dots are those rays that hit before xy-mirror and after zy-mirror, the blue ones hit first xy-mirror and after zy-mirror.

4.4.3 Analysis of orthogonality

Figure 4.17 presents the interesting histograms versus the horizontal angle x' when the angle between the mirrors change ($\alpha = 90^\circ + \Delta$). It can be noted a improvement of the collimation of the beam changing the angle in the case of closer mirrors ($\Delta = -0.01^\circ$). Figure 4.16 show the trend of the FWHM of the x' changing the angle Δ , it is possible to note a minimum for negative angle (this ideal situation

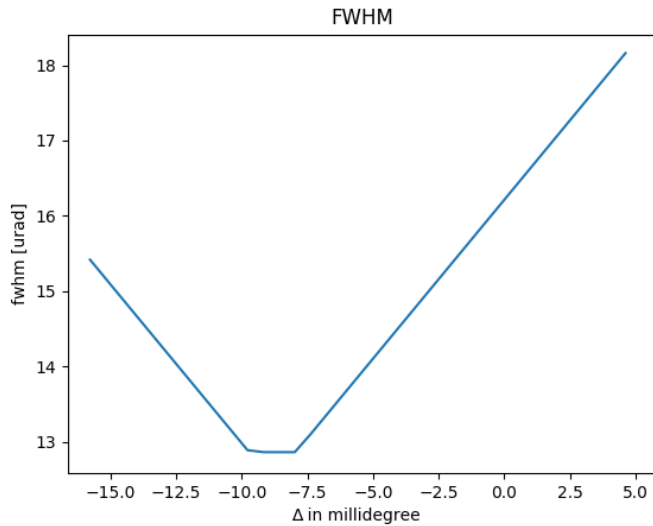
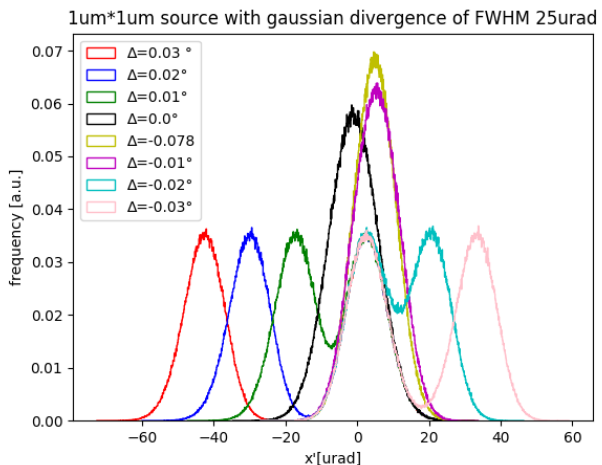


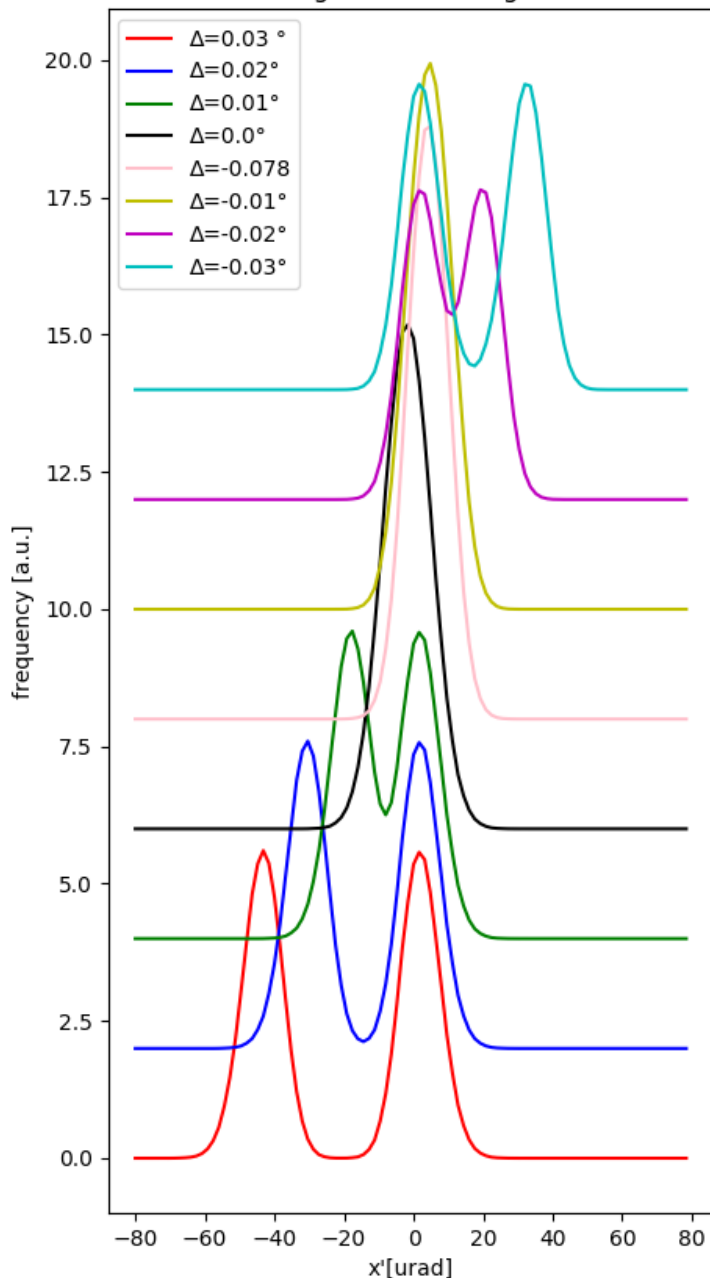
Figura 4.16: FWHM of x' after the Montel changing the orthogonality

is the pink curve reported in Figure 4.17) after that the situation become worse. Moreover, the behavior of the FWHM is not symmetrical with respect to 0° , in case of negative angle deviation the situation improve for a small range of deviation angle, after that, the trend get worse, on the opposite way, the situation get worse increasing the positive deviation angle.



(a) Real histogram

1um*1um source with gaussian divergence of FWHM 25ura



Appendice A

Table for absorption coefficients

Table A. report the X-Ray Mass Attenuation Coefficients. Material constants assumed in the present evaluations for elemental media. Values are given for the ratio of atomic number-to-mass Z/A , the mean excitation energy I , and the density ρ . Some density values are only nominal; those for $Z = 85$ and 87 were arbitrarily set to 10 in order to complete the calculations.

Z	Element		Z/A	I [eV]	Density $\frac{[g]}{[cm^3]}$
1	H	Hydrogen	0.99212	19.2	8.375E-05
2	He	Helium	0.49968	41.8	1.663E-04
3	Li	Lithium	0.43221	40.0	5.340E-01
4	Be	Beryllium	0.44384	63.7	1.848E+00
5	B	Boron	0.46245	76.0	2.370E+00
6	C	Carbon, Graphite	0.49954	78.0	1.700E+00
7	N	Nitrogen	0.49976	82.0	1.165E-03
8	O	Oxygen	0.50002	95.0	1.332E-03
9	F	Fluorine	0.47372	115.0	1.580E-03
10	Ne	Neon	0.49555	137.0	8.385E-04
11	Na	Sodium	0.47847	149.0	9.710E-01
12	Mg	Magnesium	0.49373	156.0	1.740E+00
13	Al	Aluminum	0.48181	166.0	2.699E+00
14	Si	Silicon	0.49848	173.0	2.330E+00
15	P	Phosphorus	0.48428	173.0	2.200E+00
16	S	Sulfur	0.49897	180.0	2.000E+00
17	Cl	Chlorine	0.47951	174.0	2.995E-03
18	Ar	Argon	0.45059	188.0	1.662E-03
19	K	Potassium	0.48595	190.0	8.620E-01
20	Ca	Calcium	0.49903	191.0	1.550E+00
21	Sc	Scandium	0.46712	216.0	2.989E+00
22	Ti	Titanium	0.45948	233.0	4.540E+00
23	V	Vanadium	0.45150	245.0	6.110E+00

Z	Element		Z/A	I [eV]	Density $\frac{[g]}{[cm^3]}$
24	Cr	Chromium	0.46157	257.0	7.180E+00
25	Mn	Manganese	0.45506	272.0	7.440E+00
26	Fe	Iron	0.46556	286.0	7.874E+00
27	Co	Cobalt	0.45815	297.0	8.900E+00
28	Ni	Nickel	0.47708	311.0	8.902E+00
29	Cu	Copper	0.45636	322.0	8.960E+00
30	Zn	Zinc	0.45879	330.0	7.133E+00
31	Ga	Gallium	0.44462	334.0	5.904E+00
32	Ge	Germanium	0.44071	350.0	5.323E+00
33	As	Arsenic	0.44046	347.0	5.730E+00
34	Se	Selenium	0.43060	348.0	4.500E+00
35	Br	Bromine	0.43803	343.0	7.072E-03
36	Kr	Krypton	0.42959	352.0	3.478E-03
37	Rb	Rubidium	0.43291	363.0	1.532E+00
38	Sr	Strontium	0.43369	366.0	2.540E+00
39	Y	Yttrium	0.43867	379.0	4.469E+00
40	Zr	Zirconium	0.43848	393.0	6.506E+00
41	Nb	Niobium	0.44130	417.0	8.570E+00
42	Mo	Molybdenum	0.43777	424.0	1.022E+01
43	Tc	Technetium	0.43919	428.0	1.150E+01
44	Ru	Ruthenium	0.43534	441.0	1.241E+01
45	Rh	Rhodium	0.43729	449.0	1.241E+01
46	Pd	Palladium	0.43225	470.0	1.202E+01
47	Ag	Silver	0.43572	470.0	1.050E+01
48	Cd	Cadmium	0.42700	469.0	8.650E+00
49	In	Indium	0.42676	488.0	7.310E+00
50	Sn	Tin	0.42120	488.0	7.310E+00
51	Sb	Antimony	0.41889	487.0	6.691E+00
52	Te	Tellurium	0.40752	485.0	6.240E+00
53	I	Iodine	0.41764	491.0	4.930E+00
54	Xe	Xenon	0.41130	482.0	5.485E-03
55	Cs	Cesium	0.41383	488.0	1.873E+00
56	Ba	Barium	0.40779	491.0	3.500E+00
57	La	Lanthanum	0.41035	501.0	6.154E+00
58	Ce	Cerium	0.41395	523.0	6.657E+00
59	Pr	Praseodymium	0.41871	535.0	6.710E+00
60	Nd	Neodymium	0.41597	546.0	6.900E+00
61	Pm	Promethium	0.42094	560.0	7.220E+00
62	Sm	Samarium	0.41234	574.0	7.460E+00
63	Eu	Europium	0.41457	580.0	5.243E+00
64	Gd	Gadolinium	0.40699	591.0	7.900E+00
65	Tb	Terbium	0.40900	614.0	8.229E+00
66	Dy	Dysprosium	0.40615	628.0	8.550E+00
67	Ho	Holmium	0.40623	650.0	8.795E+00
68	Er	Erbium	0.40655	658.0	9.066E+00
69	Tm	Thulium	0.40844	674.0	9.321E+00
70	Yb	Ytterbium	0.40453	684.0	6.730E+00
71	Lu	Lutetium	0.40579	694.0	9.840E+00

Z	Element		Z/A	I [eV]	Density $\frac{[g]}{[cm^3]}$
72	Hf	Hafnium	0.40338	705.0	1.331E+01
73	Ta	Tantalum	0.40343	718.0	1.665E+01
74	W	Tungsten	0.40250	727.0	1.930E+01
75	Re	Rhenium	0.40278	736.0	2.102E+01
76	Os	Osmium	0.39958	746.0	2.257E+01
77	Ir	Iridium	0.40058	757.0	2.242E+01
78	Pt	Platinum	0.39984	790.0	2.145E+01
79	Au	Gold	0.40108	790.0	1.932E+01
80	Hg	Mercury	0.39882	800.0	1.355E+01
81	Tl	Thallium	0.39631	810.0	1.172E+01
82	Pb	Lead	0.39575	823.0	1.135E+01
83	Bi	Bismuth	0.39717	823.0	9.747E+00
84	Po	Polonium	0.40195	830.0	9.320E+00
85	At	Astatine	0.40479	825.0	1.000E+01
86	Rn	Radon	0.38736	794.0	9.066E-03
87	Fr	Francium	0.39010	827.0	1.000E+01
88	Ra	Radium	0.38934	826.0	5.000E+00
89	Ac	Actinium	0.39202	841.0	1.007E+01
90	Th	Thorium	0.38787	847.0	1.172E+01
91	Pa	Protactinium	0.39388	878.0	1.537E+01
92	U	Uranium	0.38651	890.0	1.895E+01

Appendice B

How to calculated the ellipse's and hyperbola's coefficients

For the ellipse showed in Figure B.1, the ellipse is defined as:

$$\left(\frac{x'}{a}\right)^2 + \left(\frac{y'}{b}\right)^2 = 1 \quad (\text{B.1})$$

with

$$c^2 = a^2 - b^2 \quad (\text{B.2})$$

Because the ellipse is the curve in a plane surrounding two focal points such that the sum of the distances to the two focal points is constant for every point, so:

$$p + q = (c + a) + (a - c) = 2a \quad (\text{B.3})$$

Thus

$$a = \frac{p + q}{2} \quad (\text{B.4})$$

Now, considering the triangle $AA'P$, using the law of cosines, and substituting with the equations above:

$$4c^2 = p^2 + q^2 - 2pq\cos(2\vartheta) \quad (\text{B.5})$$

$$4(a^2 - b^2) = p^2 + q^2 - 2pq\cos(2\vartheta) \quad (\text{B.6})$$

$$(p + q)^2 - 4b^2 = p^2 + q^2 - 2pq\cos(2\vartheta) \quad (\text{B.7})$$

$$b^2 = \frac{2pq(1 + \cos(2\vartheta))}{4} \quad (\text{B.8})$$

$$b = \sqrt{pq}\cos(\vartheta) \quad (\text{B.9})$$

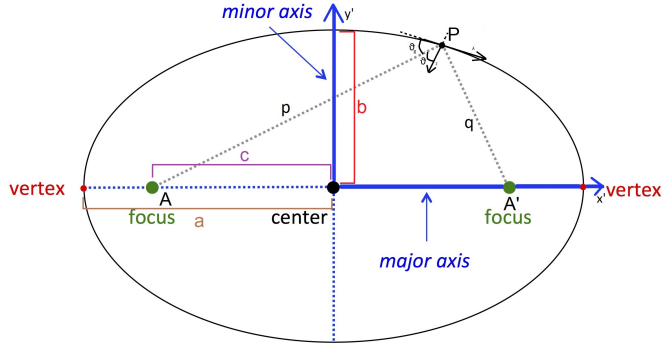


Figura B.1: Hyperbola's system

For the Hyperbola the situation is similar. For the system in Figure B.2, the equation of the parabola is

$$\left(\frac{x'}{a}\right)^2 - \left(\frac{y'}{b}\right)^2 = 1 \quad (\text{B.10})$$

with

$$c^2 = a^2 + b^2 \quad (\text{B.11})$$

In this case the definition of hyperbola is the curve in a plane surrounding two focal points such that the difference of the distances to the two focal points is constant for every point, so:

$$p - q = (c + a) - (c - a) = 2a \quad (\text{B.12})$$

Thus

$$a = \frac{p - q}{2} \quad (\text{B.13})$$

As before, considering the triangle F_1F_2P , using the law of cosines, and substituting with the equations above:

$$4c^2 = p^2 + q^2 - 2pq\cos(2\vartheta_g) \quad (\text{B.14})$$

$$4(a^2 + b^2) = p^2 + q^2 - 2pq\cos(2\vartheta_g) \quad (\text{B.15})$$

$$(p - q)^2 + 4b^2 = p^2 + q^2 - 2pq\cos(2\vartheta_g) \quad (\text{B.16})$$

$$b^2 = \frac{2pq[1 - \cos(2\vartheta_g)]}{4} \quad (\text{B.17})$$

$$b = \sqrt{pq}\sin(\vartheta_g) = \sqrt{pq}\cos(\vartheta_g) \quad (\text{B.18})$$

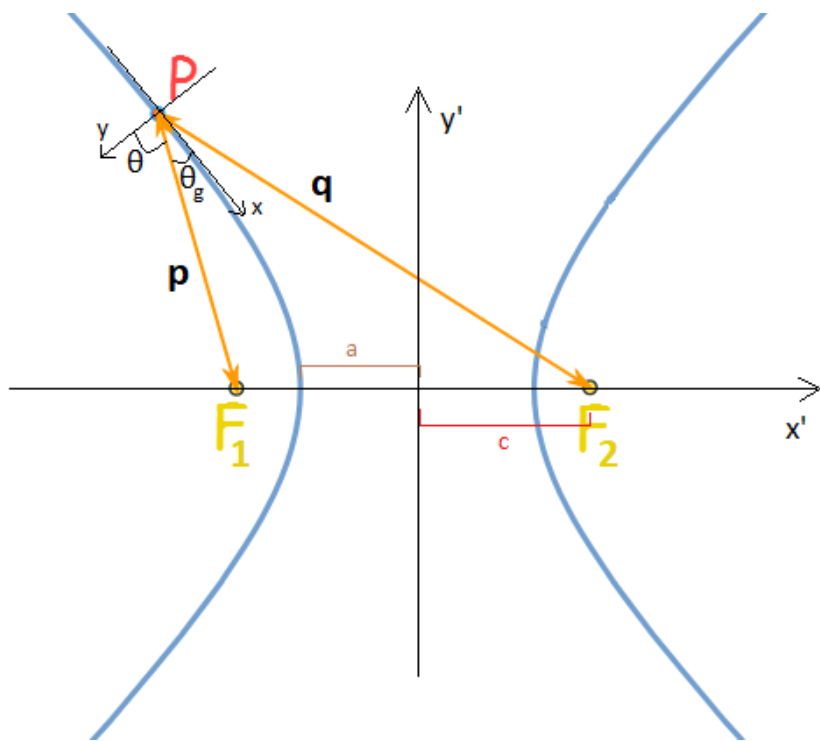


Figura B.2: Hyperbola's system

Bibliografia

- [Aga91] Bipin K Agarwal. Interaction of x-rays with matter. In *X-Ray Spectroscopy*, pages 121–126. Springer, 1991.
- [BAR11] Ray BARRETT. X-ray optics for synchrotron radiation beamlines. Presentation of Ray Barrett on his work at ESRF presented at ESI2011: 2nd EIROforum School on Instrumentation, 2011.
- [CL70] Don T Cromer and David Liberman. Relativistic calculation of anomalous scattering factors for x rays. *The Journal of Chemical Physics*, 53(5):1891–1898, 1970.
- [Dal16] Daniele Dallacasa. Processi di radiazione e mhd, 2016.
- [Fit06] Richard Fitzpatrick. Rayleigh scattering, 2006.
- [FTGY⁺00] Robert Edward Fischer, Biljana Tadic-Galeb, Paul R Yoder, Ranko Galeb, Bernard C Kress, Stephen C McClain, Tom Baur, Richard Plympton, Bob Wiederhold, and Bob Grant Alastair J. *Optical system design*. Citeseer, 2000.
- [GHJV95] Erich Gamma, Richard Helm, Ralph Johnson, and John Vlissides. *Design patterns: Abstraction and reuse of object-oriented design*. Springer, 1995.
- [gis15] gisaxs. Refractive index, 2015.
- [HHK⁺10] Marcelo Goncalves Honnicke, Xianrong Huang, Jeffrey W Keister, Chaminda Nalaka Kodituwakku, and Yong Q Cai. Tracing x-rays through an l-shaped laterally graded multilayer mirror: a synchrotron application. *Journal of synchrotron radiation*, 17(3):352–359, 2010.
- [IBK09] Gene E Ice, Rozaliya I Barabash, and Ali Khounsary. Nested mirrors for x-rays and neutrons. In *Advances in X-Ray/EUV Optics and Components IV*, volume 7448, page 74480B. International Society for Optics and Photonics, 2009.
- [LBN10] MSD LBNL. Center for x-ray optics, 2010.
- [LIA⁺11] Wenjun Liu, Gene E Ice, Lahsen Assoufid, Chian Liu, Bing Shi, Ruben Khachtryan, Jun Qian, Paul Zschack, Jonathan Z Tischler, and J-Y Choi. Achromatic nested kirkpatrick–baez mirror optics for hard x-ray nanofocusing. *Journal of synchrotron radiation*, 18(4):575–579, 2011.

- [Man81] Steven T Manson. Theory of sub-kev photoionization cross sections. In *AIP Conference Proceedings*, volume 75, pages 156–161. AIP, 1981.
- [Mic86] A.G. Michette. *Optical systems for soft X rays*. Plenum Press, 1986.
- [Mon57] M i Montel. X-ray microscopy with catamegonic roof mirrors. *X-ray Microscopy and Microradiography*, pages 177–185, 1957.
- [MSL⁺14] K Mundboth, J Sutter, D Laundy, S Collins, S Stoupin, and Yu Shvyd'ko. Tests and characterization of a laterally graded multilayer montel mirror. *Journal of synchrotron radiation*, 21(1):16–23, 2014.
- [MY09] S Matsuyama and H Yumoto. Textbook for hard x-ray focusing with kirkpatrick-baez optics. *Unpublished Report*, 2009.
- [RKM15] Giacomo Resta, Boris Khaykovich, and David Moncton. Nested kirkpatrick-baez (montel) optics for hard x-rays. *Journal of Applied Crystallography*, 48(2):558–564, 2015.
- [SFV09] Francesc Salvat and José Fernández-Varea. Overview of physical interaction models for photon and electron transport used in monte carlo codes. *Metrologia*, 46:S112, 03 2009.
- [Sin11] Kulinder Pal Singh. Grazing incidence optics for x-ray astronomy. *Journal of Optics*, 40(3):88, 2011.
- [SS05] Robert Shannon and Roland Shack. *Legends in Applied Optics*. James E. Harvey, 2005.
- [Uni16] Boston University. *Compton Scattering*, 2016.
- [Wik18] Wikipedia. Parabola (geometria). 2018. [Online; accessed 1-December-2018].